

# Nebulized fusion inhibitory peptide protects cynomolgus macaques from measles virus infection

**Olivier Reynard**

International Center for Infectiology Research <https://orcid.org/0000-0001-7536-355X>

**Claudia Gonzalez**

INSERM

**Claire Dumont**

INSERM <https://orcid.org/0000-0001-7511-1512>

**Mathieu Iampietro**

CIRI, Centre International de Recherche en Infectiologie <https://orcid.org/0000-0002-8946-3049>

**Marion Ferren**

Columbia University Medical Center

**Sandrine Le Guellec**

DTF-Aerodrug

**Laurie Lajoie**

Université de Tours, EA 7501 GICC <https://orcid.org/0000-0001-7299-6407>

**Cyrille Mathieu**

CIRI, Centre International de Recherche en Infectiologie, Team Immuno-Biology of Viral Infections, Univ Lyon, Inserm, U1111, Université Claude Bernard Lyon 1, CNRS, UMR5308, ENS de Lyon

<https://orcid.org/0000-0002-6682-2029>

**Gabrielle Carpentier**

Université de Tours

**Georges Roseau**

Université de Tours

**Francesca Bovier**

Columbia University Medical Center

**Yun Zhu**

Columbia University

**Deborah Le Pennec**

INSERM

**Jerome Montharu**

Université de Tours

**Amin Addetia**

University of Washington Med center

**Alexander Greninger**

University of Washington

**Christopher Alabi**

Cornell University <https://orcid.org/0000-0003-2654-018X>

**Anne Moscona**

Columbia University Medical Center <https://orcid.org/0000-0002-1796-8320>

**Laurent Vecellio**

Université de Tours

**Matteo Porotto**

Columbia University Medical Center <https://orcid.org/0000-0003-3866-9220>

**Branka Horvat** (✉ [branka.horvat@inserm.fr](mailto:branka.horvat@inserm.fr))

INSERM <https://orcid.org/0000-0003-0578-7765>

---

## Article

### Keywords:

**Posted Date:** June 1st, 2022

**DOI:** <https://doi.org/10.21203/rs.3.rs-1700877/v1>

**License:**   This work is licensed under a Creative Commons Attribution 4.0 International License.

[Read Full License](#)

---



27 <sup>9</sup> Robert Frederick Smith School of Chemical and Biomolecular Engineering, Cornell University,  
28 Ithaca, New York, USA

29 <sup>10</sup> Department of Microbiology and Immunology, Columbia University Vagelos College of  
30 Physicians & Surgeons, New York, NY, USA.

31 <sup>11</sup> Department of Physiology & Cellular Biophysics, Columbia University Vagelos College of  
32 Physicians & Surgeons, New York, NY, USA.

33 <sup>12</sup> Department of Experimental Medicine, University of Studies of Campania 'Luigi Vanvitelli',  
34 Naples, Italy.

35

36

37 **Address correspondence to:**

38 Branka Horvat, CIRI, 21 Avenue Tony Garnier, 69007 Lyon, France, tel: +33 4 3728 2392, Email:  
39 [branka.horvat@inserm.fr](mailto:branka.horvat@inserm.fr)

40

41

42 **Abstract:**

43 Measles is the most contagious airborne viral infection and the leading cause of child death among  
44 vaccine-preventable diseases. We show here that aerosolized lipopeptide fusion inhibitors, derived  
45 from heptad-repeat regions of the measles virus (MeV) fusion protein, block respiratory MeV  
46 infection in a non-human primate model, the cynomolgus macaque. We used a custom-designed  
47 mesh nebulizer to ensure efficient aerosol delivery of peptides to the respiratory tract and  
48 demonstrated the absence of adverse effects and lung pathology in macaques. The nebulized  
49 peptide efficiently prevented MeV infection, resulting in the complete absence of MeV RNA,  
50 MeV-infected cells, and MeV-specific humoral responses in treated animals. This strategy  
51 provides an additional shield which complements vaccination to fight against respiratory infection,  
52 presenting a proof-of-concept for the aerosol delivery of fusion inhibitory peptides to protect  
53 against measles and other airborne viruses, including SARS-CoV-2, in case of high-risk exposure,  
54 that can be readily translated to human trials.

55

## 56 INTRODUCTION

57 Measles virus (MeV), a member of the *Paramyxoviridae* family of single-stranded negative sense  
58 RNA viruses, is one of the most infectious microorganisms worldwide, with a primary  
59 reproduction rate of 12-18<sup>1</sup>. Despite the availability of a safe and effective vaccine, measles causes  
60 3 to 4 million cases annually, claimed 207.500 lives in 2019, and remains a leading cause of  
61 childhood death from vaccine-preventable diseases in many developing countries<sup>2</sup>. Although  
62 incidence has decreased considerably from 2000 to 2016 (from 145 to 18 per million), measles has  
63 increased since 2017<sup>2</sup> and is expected to further increase in incidence as a result of the SARS-  
64 CoV-2 pandemic and the intercurrent delays in childhood immunization programs and resultant  
65 “immunity gaps” in the population<sup>3-6</sup>. In addition, in developed countries, imported outbreaks  
66 pose a significant risk for immunocompromised people who rely on herd immunity and cannot  
67 receive the current live vaccine<sup>7</sup>.

68 MeV is an airborne pathogen, transmitted by inhalation of respiratory droplets and smaller  
69 aerosol. Initial infection targets susceptible cells in the respiratory tract<sup>8,9</sup>. After an incubation  
70 period of 7 to 10 days, the acute phase is characterized by fever, oculo-respiratory inflammation,  
71 cough, and Koplick spots<sup>10</sup>. The characteristic erythematous skin rash occurs around 14 days after  
72 infection<sup>11</sup> when MeV infects cells in the epidermis<sup>11,12</sup>. MeV is amplified in regional lymphoid  
73 tissues, followed by systemic infection when MeV-infected lymphocytes and dendritic cells (DCs)  
74 migrate into the subepithelial cell layers and transmit MeV to the epithelial cells of various  
75 tissues<sup>13</sup>. After amplification of MeV in the epithelia, progeny virus is released into the respiratory  
76 tract, either free or as dislodged infectious centers consisting of infected cells<sup>14</sup>. Infection generally  
77 resolves after three weeks, but is often followed by immune suppression which may last for several  
78 months and is responsible for numerous complications associated with measles<sup>15,16</sup>. Rare but  
79 severe complications of measles involve central nervous system infection progressing to lethal  
80 MeV encephalitis<sup>7</sup>.

81 MeV uses several receptors to infect target cells. The virus binds to CD150 (SLAMF1,  
82 SLAM) to infect macrophages, DCs, and lymphocytes<sup>17</sup>, and the attachment is aided by the CD209  
83 (DC-SIGN) co-receptor<sup>18,19</sup>. Alternatively MeV can use nectin-4 as an attachment factor to infect  
84 the basolateral side of the epithelial airway, a process that promotes viral dissemination<sup>20,21</sup>. Recent  
85 data suggest that entry may also occur from the apical side of the airway in a nectin-4-independent

86 manner<sup>8,9</sup>. Finally, a role for CADM1 and 2 in neuroinvasion has been postulated<sup>22</sup>. Infection is  
87 initiated following the attachment of the hemagglutinin (H) protein to one of MeV receptors; H  
88 then activates the fusion protein (F), and the ensuing rearrangement of F promotes insertion of the  
89 hydrophobic fusion peptide into the facing cellular membrane. A second folding event occurs  
90 driven by interaction between N- and C- terminal heptad repeat (HR) regions (HRC and HRN  
91 domains respectively) of F, completing virus-cell membrane fusion<sup>23</sup>. Our previous work has  
92 demonstrated that peptides derived from HRC region can interfere with the second folding event  
93 required for virus-to-cell fusion during MeV infection<sup>24,25</sup>. A dimerized version of a peptide  
94 corresponding to the HRC region, conjugated to a cholesterol moiety (referred to as “HRC4”  
95 peptide, Fig. 1D), inhibited the fusion process in cell culture and in organotypic brain cultures<sup>24</sup>.  
96 HRC4 peptide administered intranasally to cotton rats and to humanized transgenic mouse models  
97 of lethal measles disease led to reduction of the viral titer in cotton rat lungs and a significant  
98 increase in survival of mice <sup>24,25</sup>.

99 Advantages of inhaled protein therapeutics include the non-invasive needle-free drug  
100 delivery route, and the ease of depositing drugs directly in the lungs while limiting systemic  
101 toxicity<sup>26</sup>. Since the approval of inhaled Dornase alfa for treating pulmonary disease in cystic  
102 fibrosis, several peptides have been under clinical development for inhaled delivery<sup>27</sup>. Nebulizers  
103 can be used for high dose delivery with limited drug formulation development<sup>26-28</sup>. In the present  
104 study, a mesh nebulizer was used to deliver MeV fusion inhibitory peptides to nonhuman primates  
105 (NHPs) – cynomolgus macaques – a well-characterized model that recapitulates measles infection  
106 in humans<sup>29</sup>. The mesh nebulizer applied in this study uses a piezo-electric generator to push the  
107 drug solution through a micro-perforated metal sieve, allowing a fast and silent drug delivery <sup>28</sup>.  
108 Small diameters of the sieve pores generate aerosols smaller than 5 µm, enabling efficient  
109 pulmonary drug delivery<sup>27</sup>. Using this mesh nebulizer for respiratory administration of fusion  
110 inhibitory peptide we effectively inhibit MeV infection in the macaque model. These results open  
111 novel perspectives for antiviral prevention strategy against measles and possibly other airborne  
112 viruses, including SARS-CoV-2.

113

114

115

## 116 RESULTS

### 117 Treatment with HRC4 lipopeptide does not promote selection of drug-resistant variants

118 Generation of escape variants is a concern with any antiviral<sup>30</sup>, we initially tested for emergence  
119 of peptide resistant MeV variants in cell culture. Recombinant MeV IC323-eGFP<sup>31</sup> was grown on  
120 Vero-hSLAM cells in the presence of either 1  $\mu$ M HRC4 peptide or another fusion inhibitory  
121 peptide (FIP) carbobenzoxy-(Z)-D-Phe-L-Phe-Gly peptide<sup>32</sup>, -[FIP-PEG<sub>4</sub>]<sub>2</sub>-Chol- which was  
122 dimerized and coupled to cholesterol like HRC4<sup>33</sup>. Viruses were sequenced after eight passages  
123 (Fig. 1a). In the [FIP-PEG<sub>4</sub>]<sub>2</sub>-Chol-treated cells, two mutations in MeV HRC domain were  
124 identified, in the same residues as described previously under the selective pressure of the  
125 unconjugated FIP, V<sub>459</sub> and N<sub>462</sub><sup>34</sup> (Fig. 1a, b). However, no mutations were identified in the  
126 HRC4-treated MeV. The FIP resistant MeV variants were susceptible to inhibition by HRC4  
127 peptide, as determined using a quantitative fusion assay (Fig. 1c). Fusion between cells expressing  
128 wt or variant MeV glycoproteins and cells expressing hSLAM was measured by  $\beta$ -galactosidase  
129 complementation in the presence of 5  $\mu$ M of FIP or HRC4. FIP inhibited membrane fusion  
130 mediated by the wild-type F and F-V<sub>459</sub>I but did not affect the fusion mediated by F-N<sub>462</sub>S or F-  
131 N<sub>462</sub>S/V<sub>459</sub>I mutated proteins. In contrast, HRC4 inhibited membrane fusion mediated by the wild-  
132 type and mutant F proteins (Fig. 1c). These data demonstrated the absence of HRC4-resistant MeV  
133 mutants following multiple viral passages and strengthen the selection of HRC4 lipopeptide (Fig.  
134 1d) for further preclinical development of MeV fusion inhibitory peptide.

135

### 136 Analysis of the dose and schedule of HRC4 administration in murine model of MeV infection

137 We next evaluated the dose and schedule of HRC4 peptide by intranasal administration in the  
138 humanized murine transgenic model of CD150xIFN $\alpha$ / $\beta$ R KO mice, previously shown to be very  
139 susceptible to MeV intranasal infection<sup>35,36</sup>. Mice were treated with HRC4 peptide (1 or 0.1 mg/kg)  
140 either twenty-four or six hours prior to intranasal infection with a lethal dose of MeV-IC323-eGFP  
141 ( $10^4$  PFU). All mock-treated mice succumbed to the infection by day 12 post-infection (p.i.), while  
142 the treatment with the HRC4 (1 mg/kg) six and twenty-four hours before infection led to a  
143 significantly higher survival rate ( $p < 0.0001$ , Mantel-Cox test) (Fig. S1).

144 Based on these results and previous work<sup>25,37</sup>, we selected for further studies a 4 mg/kg  
145 dose, given 3 times by nebulization, 24 h and 6 h before infection, and 24 h after infection, to

146 optimize the antiviral effect of HRC4 in primates which are highly susceptible to MeV, considering  
147 the possible loss of peptide delivered through nebulization. This choice was also driven by a  
148 recently published study of the therapeutic three-time nebulization of antiviral compound in  
149 respiratory syncytial virus (RSV)-infected children<sup>38</sup>.

150

### 151 **Characterization of an aerosol device for lipopeptide delivery into the lung alveoli**

152 MeV infection of the respiratory tract targets the lung alveoli<sup>8</sup>, we therefore engineered an inhaled  
153 strategy and used a customized mesh nebulizer to deliver the HRC4 lipopeptide aerosol deep into  
154 the respiratory tract, to block virus infection. The particle size measurement of aerosol generated  
155 following the nebulization of either HRC4 peptide or saline solution (0.9% NaCl) using a prototype  
156 mesh nebulizer with a 3  $\mu\text{m}$  pore sieve and a prototype face mask (Fig. 2a) was assessed by laser  
157 diffraction (Fig. 2b). The nebulizer devices delivered particles with an average size of 4  $\mu\text{m}$ , in  
158 terms of the Volume Mean Diameter (VMD), of both peptide and saline solution, at a flow rate of  
159 0.32 - 0.46 ml/min (Fig. 2b, detailed in Table S1). Approximately 58% of particles were smaller  
160 than 5 $\mu\text{m}$ , which is the aerosol size that reaches the airways<sup>27</sup>, where MeV infection initiates.

161 The inhibitory effects of HRC lipopeptide *in vitro* were evaluated before and after  
162 nebulization to address the possibility that nebulization itself could inducing aggregation or  
163 degradation of peptide with resultant loss of activity<sup>26,27</sup> (Fig. 2c and d). Nebulization of HRC4  
164 did not cause any loss of activity. Cytotoxicity of the nebulized HRC4 before and after nebulization  
165 was evaluated *in vitro* using Vero-E6 cells (Fig. 2d). No measurable cytotoxicity was observed at  
166 doses ranging from 0.5 nM to 4  $\mu\text{M}$ , indicating that the HRC4 therapeutic index is higher than 500  
167 (4 $\mu\text{M}$  / 8nM)<sup>39</sup>.

168

### 169 **Biodistribution and safety of nebulized HRC4 in cynomolgus macaques**

170 Delivery of aerosol by the customized nebulizer to the macaques was measured by scintigraphy  
171 imaging of animals nebulized with <sup>99m</sup>Tc-DTPA-labeled in NaCl 0.9% solution, chosen since  
172 HRC4 peptide solution and NaCl shared similar aerodynamic properties (Table S1). After  
173 nebulization, 40% of the total aerosolized product reached the respiratory tract, with 11.4%  
174 distributed into the lungs (Fig. 3a). The deposition of the HRC4 peptide in the respiratory tract was



175 further analyzed using anti-HRC4 antibodies for the immunofluorescent detection of the peptides  
176 in lungs of macaques, sampled either immediately after nebulization (15 min) or 16 h and 24 h  
177 later (Fig. 3b and S2). As expected from the scintigraphy imaging, analysis of all three lung regions  
178 revealed the presence of HRC4 within the alveoli surface area, suggesting peptide distribution  
179 throughout the lungs following the nebulization.

180 We further analyzed whether peptide could reach the blood circulation following the  
181 nebulization. HRC4 was found in low concentration (below 1nM) in the serum of nebulized  
182 animals, up to 96 h after a third nebulization (Fig. 3c), while it was absent in the urine. Low entry  
183 of the peptide into the circulation did not lead to the active immunization of animals, as HRC4  
184 specific antibodies were not found in the serum 28 days after nebulization (Fig. 3d). In addition,  
185 no adverse effects (pyrexia, allergic reaction) were observed during the 28 days after peptide  
186 nebulization. Histological analysis of lungs collected from nebulized animals did not reveal any  
187 abnormalities (Fig. S3).

188 Biochemical parameters in the plasma and cellular composition of the blood were  
189 evaluated immediately before treatment and 1, 2, 3, 6, and 28 days after nebulization of either  
190 saline or HRC4 peptide in non-infected and MeV-infected NHP, to search for early and late toxic  
191 effects of the aerosol delivery (Fig. 4). Analysis of the numerous hematological and biochemical  
192 parameters in noninfected animals did not show significant variations between groups. In both  
193 control and peptide group, few animals experienced transient increase of creatine kinase over  
194 physiological values<sup>40</sup> (Fig. 4a) which can be linked to intramuscular anesthesia<sup>41</sup>. In addition,  
195 flow cytometry monitoring of the composition of major PBMC populations in blood did not reveal  
196 any significant changes in animals nebulized with peptides compared to values obtained before the  
197 nebulization (Fig. S6).

198

### 199 **Modelling of the virus and peptide deposition on the lung surface area**

200 To estimate the coverage of the lung surface area of a NHP following the aerosolization of a  
201 peptide present within the nebulised particles, in the relationship to the administrated viral  
202 inoculum, we performed the mathematical modelling, schematically presented in the Fig. 5. The  
203 estimation is based on the calculation of either virus or peptide dose per unit of lung surface as  
204 described in the FDA guidance for inhalation product<sup>42</sup>. The calculation took into consideration

205 the number of droplets formed following the administration, the distribution of viral particles and  
 206 the amount of peptide molecules covering the pulmonary area <sup>43</sup>. Calculation of the number of  
 207 infectious viral particles (N<sub>v</sub>) administrated in the macaque's lung took into account the method  
 208 of viral administration which consists in delivering 10000 plaque-forming unit (PFU) of virus,  
 209 (N<sub>v</sub>) in a form of liquid (V<sub>v</sub>), through the endo-tracheal tube, leading to the formation of the thin  
 210 liquid layer in the lung conductive airways<sup>44</sup>. Taking into account the worst-case scenario, ie a  
 211 liquid thickness (T<sub>v</sub>) of 7 μm<sup>45</sup> recovering the epithelia in the conductive airways, we calculated  
 212 the surface (S<sub>v</sub>) covered by the 5 ml liquid volume (2 ml inoculum and 3 ml washout):

$$213 \quad S_v = V_v / T_v = \mathbf{7140 \text{ cm}^2}$$

214 Then, the calculation of the virus concentration (C<sub>v</sub>) in the region of infected surface lung  
 215 was performed using the following formula:

$$216 \quad C_v = N_v / S_v = \mathbf{1.4 \text{ PFU/cm}^2}$$

217 Determination of the number of droplets administrated in the macaque lung was based on  
 218 results presented in the Fig. 2A, showing that the deposition fraction in the lung (E) is around 10%,  
 219 with the nebulizer charge V<sub>p</sub> = 3ml, giving thus 0.3 ml in a form of deposited droplets in the lung.  
 220 Knowing the mean diameter of droplets (D<sub>p</sub> = 4 μm), we can calculate the number of deposited  
 221 droplets (N<sub>d</sub>) as follows:

$$222 \quad \text{particles volume} = \frac{4 \pi}{3} \left(\frac{D_p}{2}\right)^3$$

$$223 \quad N_d = \frac{E V_p}{\text{particles volume}} = \frac{6 E V_p}{\pi D_p^3} = \mathbf{9 \times 10^9 \text{ droplets}}$$

224 Based on the peptide concentration (400 nmol/ml) and the nebulizer charge (V<sub>p</sub>), we can  
 225 calculate the number of peptide (N<sub>p</sub>) deposited in the lung as follow:

$$226 \quad N_p = N_a C_m V_p E = \mathbf{7 \times 10^{16} \text{ peptide molecules}} \quad (N_a: \text{Avogadro number})$$

227 If we consider a homogenous deposition of the liquid in the lungs, we can calculate the  
 228 concentration in terms of number of peptide molecules per surface of lung as the ratio of the  
 229 number of peptide molecules (N<sub>p</sub>) and the macaque's lung surface:

$$230 \quad [R] = \frac{N_p}{\text{alveoli area} \times \text{total number of alveoli}} = \frac{7.22 \times 10^{16}}{(0.19 \text{mm}^2 \times (2 \times 57.8,106))} = \mathbf{3 \times 10^{11} \text{ peptide /cm}^2}$$

231           Consequently, in the lung of the macaque, a surface of 7140 cm<sup>2</sup> was covered with the  
232 virus 1.4 PFU / cm<sup>2</sup>. On the same lung surface, we deposited by nebulisation 3x10<sup>11</sup> peptide/cm<sup>2</sup>.  
233 This concentration of peptide was administrated homogeneously to the totality of the lung.  
234 Interestingly, we have obtained a 2x10<sup>11</sup> ratio between the peptide and the virus per cm<sup>2</sup> in the  
235 infected lung surface, being thus largely in favor of the peptide deposition (Fig. 5), and highly  
236 encouraging for the further *in vivo* assay using MeV infected NHP.

237           Finally, when the estimation of the peptide and virus deposition in the *in vitro* tissue culture  
238 was performed using a similar type of calculation, the large excess of the peptide to virus was also  
239 obtained (5x10<sup>11</sup> peptides/cm<sup>2</sup>, Fig. S4), in accord to the highly efficient inhibition of virus  
240 infection seen *in vitro* (Fig. 2c and d).

241

#### 242 **Nebulized HRC4 peptide protects cynomolgus macaques from MeV infection**

243 To assess antiviral efficacy of nebulized HRC4 peptide in NHPs, groups of 3 animals were infected  
244 with 10<sup>4</sup> PFU MeV IC323-eGFP by intra-tracheal inoculation, and either mock-treated with  
245 nebulized saline solution (C1, C2, and C3) or treated with nebulized HRC4 peptide (P1, P2, and  
246 P3) twenty-four and six hours before infection and twenty-four hours after infection (Fig. 6a). The  
247 NHPs were housed in cages accommodating two animals per cage for ethical reasons, so that one  
248 cage contained one peptide-treated and one saline-nebulized macaque. The animals were  
249 monitored for 28 days for the appearance of clinical signs, including temperature, weight, and  
250 behavior changes, none of which were observed during the experiment.

251           As in human infection, measles infection in NHPs induces a skin rash that can be followed  
252 macroscopically during infection with eGFP-encoding MeV<sup>17</sup>. Observation of the fluorescent skin  
253 rash is facilitated by utilizing a blue LED light, particularly in cynomolgus macaques where the  
254 red skin rash is less apparent than in rhesus macaques<sup>46</sup>. After infection with MeV-IC323-eGFP,  
255 skin and oral mucosa were monitored under blue light every three days post-infection (p.i.). All  
256 mock-treated animals, but no HRC4-treated animals, had a GFP-fluorescent rash (Fig. 6b-c). The  
257 fluorescent rash appeared as early as day 6 p.i. (animal C3) and lasted until day 16 (C1 and C2) or  
258 up to day 28 p.i. (C3), mainly located in the mouth (tongue, palate, gum, and chin) and skin  
259 (preferentially on armpits, groin, and back) (Fig. 6b-c).

260 MeV infects and replicates in circulating immune cells<sup>13,15</sup>. Infection of PBMCs was  
261 detected by flow cytometry on day three p.i. in animals C1 and C3, on day 6 p.i. in animal C2 and  
262 at a low level in animal P2 at day 9 p.i. (Fig. 6d, left panel). Consistent with eGFP expression,  
263 viral RNA followed a similar kinetic trajectory (Fig. 6d, central panel). Viremia lasted 9 to 16 days  
264 in mock-treated animals and 6 days in HRC4-treated animal P2. This NHP was housed in the same  
265 cage with mock-treated C3, which exhibited a high level of MeV infection and most probably  
266 transmitted it as a secondary infection to P2 after the end of the peptide treatment, confirming the  
267 high contagiousness of MeV infection. The viremia of animal C3 peaked at day 6 p.i. while animals  
268 C1 and C2 peaked at day nine p.i.. However, despite the delayed infection, animal P2 had less  
269 viremia than mock-treated animals. Oral shedding of virus was monitored by viral genome  
270 quantification in RNA extracts from throat swabs (Fig. 6d, right panel). Low levels of viral RNA  
271 were found at early time points and likely represent leftovers of the initial inoculum, while viral  
272 shedding peaked at day nine p.i. and lasted up to day 16 p.i. in saline-treated animals. Consistent  
273 with the PBMC results, viral RNA was only detected late and transiently at day 13-16 p.i. in the  
274 swabs from animal P2.

275

### 276 **HRC4 nebulization prevents MeV infection in peripheral immune cells**

277 Transient immunosuppression associated with leukopenia is a hallmark of MeV infection in  
278 humans<sup>15</sup> and is observed in MeV-infected NHPs. Hematological monitoring of MeV-infected  
279 NHPs demonstrated a transient leukopenia in the saline-treated group and at later time points in  
280 the infected animal P2, as observed in previous reports<sup>17,47</sup>, with total white blood cell and  
281 lymphocytes counts decreased on day 6 following MeV infection in saline-treated animals, but  
282 remained stable in HRC4-treated macaques (Fig. 4B and S5). Leukopenia lasted longer in saline-  
283 treated macaques (days 6-16 p.i.) compared to animal P2 (days 9-13 p.i.). In infected saline-treated  
284 animals, leukopenia was associated with lymphopenia, which was not observed in the fully  
285 protected macaques P1 and P3 (Fig. S5).

286 Flow cytometry studies revealed a transient decrease in B cells (CD20<sup>+</sup>) between day 9-13  
287 p.i. in mock-treated MeV-infected animals (Fig. S6). The proportion of CD3<sup>+</sup>CD4<sup>+</sup> and CD3<sup>+</sup>CD8<sup>+</sup>  
288 T cells remained unchanged (Fig. S6) despite a decrease in absolute lymphocyte number (Fig. S6).  
289 Evaluation of MeV-infected cell phenotype showed only a few CD14<sup>+</sup> monocytes positive for GFP

290 between day 6 and 13 p.i, with CD4<sup>+</sup> T lymphocytes and CD20<sup>+</sup> B lymphocytes constituting the  
291 main targets of the virus (Fig. 7a). Of the total cells infected, 40-60% were T cells and 20% were  
292 B cells, with a peak of infection day 6 (C3) or day 9 (C1, C2 and P2) p.i.. The magnitude of  
293 infection of CD3<sup>+</sup>CD8<sup>+</sup> T cells and CD14<sup>+</sup> monocytes was lower (Fig. 7a) and the majority of  
294 infected cells among PBMCs were CD4<sup>+</sup> lymphocytes (Fig. 7b). Interestingly, peptide-treated  
295 animal P2, who likely was infected later by transmission from its non-treated cage-mate, had a  
296 very low percentage of all infected cell populations, ranging between 5-30 times lower than saline-  
297 treated animals, suggesting an anti-viral effect of HRC4 nebulization followed by secondary  
298 infection from the co-housed actively infected C3 macaque (Fig. 7a).

299

### 300 **Humoral immune response in animals combatting MeV infection**

301 MeV infection induces life-long immunity to reinfection, characterized by the generation of a  
302 MeV-specific lymphocyte response<sup>15</sup>. We evaluated peripheral blood B cell phenotype and serum  
303 antibody responses in MeV-infected macaques using flow cytometry, to track the presence of  
304 unswitched (CD20<sup>+</sup> CD27<sup>+</sup> CD38<sup>+</sup> IgD<sup>+</sup>) memory B cells, secreting only IgM, and class-switched  
305 (CD20<sup>+</sup> CD27<sup>+</sup> CD38<sup>+</sup> IgD<sup>-</sup>) memory B cells, known to secrete IgG, IgA or IgE (Fig. 8a). Both B  
306 cell populations increased from day 3-6 p.i. and day 9 p.i, respectively, in mock-treated animals  
307 C2 and C3, although the response of C1 was much lower. The secondarily infected HRC4-treated  
308 animal P2 displayed a similar but delayed increase in both class-unswitched and -switched B cell  
309 populations. Notably, both P1 and P3 HRC4-treated animals were fully protected against MeV,  
310 and B cell populations remained stable without any noticeable increase.

311 MeV-specificity of the B cell response was further confirmed by serological analysis (Fig.  
312 8b and 8c). All saline-treated animals seroconverted after MeV infection, with a high MeV  
313 antibody titer on day 28 p.i. The secondarily infected animal P2 had a slightly lower total antibody  
314 titer (Fig. 8b). All seropositive animals secreted neutralizing antibodies with SN<sub>50</sub> values ranging  
315 between 546 and 3465 (Fig. 8c). The absence of seroconversion of HRC4-treated animals P1 and  
316 P3 correlated with the lack of viral replication and the distinct composition of lymphoid blood  
317 compartment in those animals, underlining the efficient and robust protection provided by the  
318 nebulized HRC4 lipopeptides.

319

320

321 **DISCUSSION**

322 Airborne infection is transmitted through small aerosolized particles suspended in the air and is  
323 responsible for spreading many important infectious diseases of humans and animals. In this study,  
324 we pioneered a nebulization approach to inhibit highly contagious MeV infection in the NHP  
325 model with fusion inhibitory peptides. As measles continues to present a significant health problem  
326 worldwide<sup>2</sup>, there is a need for prevention modalities in addition to vaccination for those who  
327 either cannot be vaccinated or do not respond appropriately to vaccination. In the current study,  
328 we adopted an approach based on immunovirological and technological research, to develop a  
329 drug and device that can be adapted to treat human patients. Fusion inhibitory HRC4 peptide  
330 provided complete protection to MeV challenge after delivery by nebulization. This needle-free  
331 therapy may find acceptance among people when compared to other routes of administration<sup>48-50</sup>.  
332 The production of 4 µm aerosolized particles by the device used in this study supports its use for  
333 targeting MeV and possibly other airborne viruses.

334 MeV infection of cynomolgus macaque mimics both pediatric respiratory infection  
335 physiology and mild MeV infection in humans<sup>47,51-55</sup>. Our results in this model have demonstrated  
336 that aerosol peptide administration using the prototype mesh nebulizer device results in efficient  
337 deposition of HRC4 peptide into lungs and persistence of detectable peptide twenty-four hours  
338 after the nebulization. This application of HRC4 peptide aerosol represents a promising initial step  
339 that supports its use in humans, where this device should work even better in the absence of the  
340 anatomical constraints of primates<sup>56</sup>. In addition, the excellent safety profile, absence of any  
341 adverse reaction, and non-immunogenic character of the compound following nebulized  
342 administration support the strategy for human use. Finally, in contrast to several other antiviral  
343 compounds<sup>30,34,57</sup>, repeated passage of MeV in the presence of HRC4 lipopeptide did not elicit  
344 viral escape mutants (Fig.1), suggesting that frequent administration may not promote  
345 development of drug resistant variants.

346 HRC4 peptide treatment abrogated the development of MeV infection in two out of three  
347 animals, measured by the absence of fluorescent rash, PBMC infection, viremia, viral shedding,  
348 and MeV-specific immune response. The third HRC4-treated animal (P2), housed with the mock-  
349 treated highly-infected animal C3, developed a late paucisymptomatic infection without rash,  
350 delayed and reduced viremia, low shedding, and late immune activation of B lymphocytes. Thus,

351 animal P2 might have been protected from MeV initial challenge by HRC4 aerosolization and  
352 acquired a MeV infection from animal C3 once the activity of the nebulized HRC4 decreased. This  
353 hypothesis agrees with the mode of action of HRC4 fusion inhibitor peptide, which is expected to  
354 prevent initial infection through daily administration and provide protection that is estimated to  
355 endure at least twenty-four hours. Although the approach presented in this work was not tested in  
356 humans, we applied both *in vitro* and *in vivo* models and mathematical modeling of the peptide  
357 and the virus deposition in the lungs to support future development and to predict how the drug  
358 delivery system will behave in humans.

359         Animals that experienced MeV infection developed a transient leukopenia consisting  
360 mainly of lymphopenia and moderate monocytosis. Those parameters were in accordance with  
361 previous descriptions of MeV tropism and disease course in the cynomolgus macaque<sup>47,58</sup>. The  
362 recorded infection levels were within the range of those observed by De Vries *et al.*<sup>47</sup> and slightly  
363 below those surveyed by De Swart *et al.*<sup>17</sup>. MeV-infected cells were preferentially CD3<sup>+</sup>CD4<sup>+</sup> T  
364 cells, followed by CD20<sup>+</sup> B cells, CD3<sup>+</sup>CD8<sup>+</sup> T cells, and subsequently CD14<sup>+</sup> monocytes, as  
365 previously described<sup>47</sup>. One animal (C3) experienced a faster acute infection with a detectable  
366 viremia on day 3 p.i. that peaked on day 6 p.i. lasted until day 16 p.i., while in other animals,  
367 viremia peaked at day 9.

368         Seroconversion was observed in all animals that developed MeV infection, as evidenced  
369 by the appearance of neutralizing antibodies and by the activation of B lymphocyte populations.  
370 In animals C2 and C3, class-unswitched memory B cells increased at 3-6 days p.i., while class-  
371 switched memory B cells started to appear day 9 p.i., consistent with primary IgM production  
372 followed by a switch in immunoglobulin class leading to a secondary secretion of IgG, A or E.  
373 Unexpectedly, animal C1 only displayed a minor and delayed modulation of its memory B cell  
374 populations, while both total immunoglobulins and neutralizing antibodies were produced.  
375 However, animal C1 demonstrated an unusual distribution of lymphocyte populations with B cell  
376 counts, representing 35% of PBMCs compared to 6% on average for the other animals. In line  
377 with this discrepancy, total Ig was delayed compared to the two other animals from the same group.  
378 HRC4-treated animals P1 and P3 developed neither signs of seroconversion nor immune cell  
379 activation, underlining the profound protection provided by HRC4 peptides. Despite displaying  
380 limited and delayed B cell activation following the pauci-symptomatic infection, animal P2  
381 seroconverted.

382           The last four years have witnessed a drastic increase in measles cases despite a highly  
383 effective vaccine <sup>3-6</sup>, suggesting the importance of developing an additional safe prophylactic  
384 strategy to support global MeV eradication. The approach developed here, nebulization of fusion  
385 inhibitory peptides, should be clinically applicable. A fusion inhibitory peptide inhibitor of HIV  
386 entry (enfuvirtide) has been commercialized to treat HIV-infected patients by subcutaneous  
387 administration<sup>57</sup>, and an oral fusion inhibitor for respiratory syncytial virus (prestatovir) is in  
388 clinical trials<sup>59</sup>. Our efforts over the last decade have been directed to design such an entry inhibitor  
389 approach for MeV<sup>25,37,60-62</sup>. The results presented here show that nebulization of our entry inhibitor  
390 peptides significantly reduces the clinical impact of MeV infection in NHP, providing a proof-of-  
391 concept for antiviral prophylaxis to be developed for humans. This strategy holds potential for  
392 protecting immunocompromised people who rely on herd immunity and cannot receive the current  
393 live MeV vaccine, since nebulized peptide is capable to completely halt viral infection. Protection  
394 against one of the most contagious aerosol-transmissible viral diseases<sup>1</sup> is a critical achievement,  
395 suggesting the potential of the nebulization approach for airborne enveloped viruses with similar  
396 entry pathways including SARS-CoV-2<sup>63</sup> or highly pathogenic Nipah virus<sup>65</sup>. In the case of viral  
397 evolution or the emergence of a new strain, the rapid development of a new antiviral based on a  
398 modified peptide sequence is feasible. Efficacy of nebulization as an administration route suggests  
399 that these antivirals are practical, possible, and within reach for use in the field where outbreaks  
400 occur. In parallel to vaccines, when available, and protective equipment, i.e. masks, aerosolized  
401 peptides may provide an additional shield to fight against extending outbreaks of airborne  
402 transmissible viruses, notably in case of high risk exposure like indoor high density people  
403 grouping (aircrafts, exhibitions, lectures ...). This antiviral strategy forms the basis for efficacious  
404 and timely emergency response immediately following identification of a new airborne virus  
405 which uses a similar fusion mechanism for viral entry <sup>25,33,61,63</sup>, now with the added benefit of a  
406 suitable delivery device.

407  
408  
409  
410  
411  
412



413 **METHODS**

414 **Study design**

415 The primary objective of this study was to evaluate the biodistribution, safety, and antiviral  
416 efficacy of nebulized MeV fusion inhibitory lipopeptide HRC4. The initial evaluation of the  
417 peptide dose and the administration schedule was performed in CD150xIFN $\alpha$ / $\beta$ R knock-out (KO)  
418 mice, highly susceptible to the intranasal MeV infection <sup>35</sup>, using 52 mice (31 males and 21  
419 females) separated into five groups. The study was completed using the NHP model of cynomolgus  
420 macaque, well-characterized to reproduce MeV infection similar to what is seen in humans <sup>29</sup>. In  
421 the setting of nebulization experiments with NHPs, the number of animals was minimized to 2  
422 times two macaques for the study of biodistribution, pharmacokinetics, and toxicology, two  
423 macaques to analyze scintigraphy gamma camera imaging of the aerosol delivery and to 2 groups  
424 of 3 NHPs, nebulized with either HRC4 peptide or saline as a control, all 6 infected with MeV, for  
425 the study of antiviral efficacy of the tested lipopeptide.

426

427 **Cells and virus**

428 Vero cells expressing human SLAM (Vero-hSLAM) were grown in DMEM glutamax (Thermo)  
429 supplemented with 10% fetal bovine serum (FBS), glutamine and antibiotics (100 U/mL of  
430 penicillin and 100  $\mu$ g/mL of streptomycin) in 5% CO<sub>2</sub> incubators at 37°C and were tested negative  
431 for mycoplasma spp (MycoAlerte, Lonza LT07-318). Recombinant MeV-IC323 expressing the  
432 gene encoding eGFP (MeV-IC323-eGFP) was generated using reverse genetics in 293-3-46 cells  
433 as previously described <sup>66</sup>, using the plasmid encoding MeV IC323-eGFP kindly provided by Y.  
434 Yanagi (Kyushu University, Fukuoka, Japan)<sup>31</sup>. Viral stocks were propagated and titrated on Vero-  
435 hSLAM cells.

436 Vero hSLAM cells were infected with 100 PFU of MeV IC323-eGFP, then incubated for  
437 2 h at 37°C and further treated with several concentrations of peptides to promote the emergence  
438 of escape variants. Viruses were collected after five days and passaged similarly eight times. Viral  
439 sequencing was performed using metagenomic next-generation sequencing as described  
440 previously<sup>67</sup>. Briefly, RNA was extracted from 50  $\mu$ L of culture harvest using the Quick-RNA  
441 Viral Kit (Zymo) and treated with TURBO DNase (Thermo, Fisher). cDNA was generated from  
442 the DNase-treated RNA using Superscript IV Reverse Transcriptase (Thermo, Fisher) and random  
443 hexamers (IDT), followed by second-strand synthesis via Sequenase Version 2.0 DNA

444 Polymerase. The resulting double-stranded cDNA was then purified with the DNA Clean &  
445 Concentrator Kit (Zymo). Libraries were constructed from 2µL of cDNA using Nextera XT kit  
446 (Illumina) and sequenced on 1x192 bp Illumina MiSeq runs. Sequencing reads were adapter and  
447 quality trimmed using Trimmomatic v0.38. Variants present at an allele frequency greater than  
448 10% and greater than 10x depth were identified with LAVA ([https://github.com/greninger-](https://github.com/greninger-lab/lava)  
449 [lab/lava](https://github.com/greninger-lab/lava)) using a previously sequenced MeV strain (NC\_001498) as the reference genome. All  
450 variants were manually confirmed by mapping sequencing reads to the same MeV reference strain  
451 in Geneious v11.1.4. Sequencing reads are deposited in NCBI BioProject PRJNA828179.

452

### 453 **MeV infection of mice**

454 CD150xIFN $\alpha$ / $\beta$ R KO mice<sup>35,36</sup>, generated by crossing SLAM transgenic mice into an IFN  
455 Receptor  $\alpha$ / $\beta$  deficient background, were bred at the institute's animal facility (PBES, ENS-Lyon,  
456 France) as heterozygotes for SLAM transgenes. Three to 4 weeks old mice (males and females)  
457 were infected i.n. with 10µl of MeV IC323 in both nares (10<sup>4</sup> PFU/mouse) under isoflurane  
458 anesthesia. CD150xIFN $\alpha$ / $\beta$ R KO mice were given i.n. either 0.1 or 1 mg/kg of HRC4 peptide 24  
459 h or 6 h before the infection. Control mice received the same number of administrations of the  
460 diluent. All animals were observed and weighed daily for four weeks and those showing clinical  
461 signs (neurological symptoms, ataxia, lethargy) were euthanized. The protocol was reviewed by  
462 the Regional Ethical Committee CECCAPP and approved under the agreement reference APAFIS  
463 N° 21141-2019042916294753v5.

464

### 465 **MeV infection of NHP**

466 Cynomolgus monkeys (*Macaca fascicularis*) were obtained from Bioprim® (Baziege, France).  
467 The effect of HRC4 nebulization on MeV infection in NHPs was analyzed at the BSL2 primate  
468 facility at the University of Tours, France. The experiment received approval from the French  
469 ethical committee and was performed under the agreement reference MESRN N°29992-  
470 2021022209579514. Six healthy female cynomolgus macaques, weighting 2.6-4 kg, aged 2-4  
471 years, were housed in groups of 2 animals/cage. All animals were confirmed by serology to be  
472 negative for MeV and canine distemper virus. Three macaques included in the control group (C1,  
473 C2, C3) were nebulized with 0.9% of NaCl, while the others received HRC4 nebulization (P1, P2,  
474 P3). The ethical obligation to house at least 2 NHPs together in the same cage resulted in two

475 animals from different groups, C3 and P2, being co-housed within the same cage, increasing the  
476 risk of late MeV transmission between those two animals. The experiment started after 21 days of  
477 acclimatization with the nebulization for a 10-15 min period, using a prototype mesh nebulizer,  
478 with either 3ml of peptide (4mg/ml) or saline (0.9% NaCl), 24 h and 6 h before infection, and 24  
479 h post-infection. Animals were infected under medetomidine/xylazine anesthesia by MeV IC323-  
480 eGFP with  $10^4$  PFU in 2mL by the intra-tracheal route, and macaques were followed for 28 days  
481 before euthanasia.

482 Blood samples for hematology analyses were collected at days -1, 0, 1, 2, 3, 6, 9, 13, 16  
483 and 28. Blood samples for flow cytometry analyses were collected at days -1, 3, 6, 9, 13, 16 and  
484 28. Throat swabs were collected at days 0, 1, 2, 3, 6, 9, 13, 16 and 28, using cotton swabs. Oxygen  
485 saturation and heartbeat were monitored by a Radical-7® Pulse CO-Oximeter (Masimo) and  
486 breathing was monitored by a Dräger Primus anesthesia machine. Hematological parameters were  
487 measured on a Procyte DX (IDEXX) and biochemical parameters were evaluated on a Konelab 30  
488 (ThermoFisher). Development of fluorescent rash was followed using a FastGene Blue/Green  
489 LED Flashlight (Nippon genetics).

490

#### 491 **Study of biodistribution and toxicology in NHP**

492 In the initial study, the pharmacokinetics and toxicology of HRC4 peptide nebulization were  
493 analyzed in 2 two-year-old healthy female cynomolgus macaques, weighing 2.8 kg, at Cynbiose,  
494 Marcy l'Etoile, France, accredited by AAALAC. The protocol was approved by the Ethics  
495 Committee of VetAgro-Sup and approved under number 146 (MESR N° 2016072117544328).  
496 Animals were initially acclimatized to their designated housing room for two weeks and gradually  
497 trained during that period to remain calm when being held by the operators during manipulations  
498 (blood sampling, monitoring of body temperature) using a reward-based training regimen. Before  
499 nebulization, animals were anesthetized with ketamine (5 to 15mg/kg) and midazolam (0.5 to 1.3  
500 mg/kg) by intramuscular injection and then placed on a baby chair. Aerosols were administered  
501 through a face mask connected to the prototype mesh nebulizer (DTF-Medical, Saint-Etienne). For  
502 the pharmacokinetic phase, the aerosolized peptide was administered via the same face mask as  
503 above to anesthetized animals on day 0. Blood samples were collected for 4, 8, 24, 48, and 72 h  
504 after nebulization. The animals had a washout period of 17 days, and blood samples were collected  
505 on day 21, the day preceding the start of the toxicology phase. For the toxicology phase, the

506 nebulized peptide was administered via a face mask to anesthetized animals daily on three  
507 consecutive days (22, 23, and 24). Urine and blood samples were collected on day 25, and animals  
508 were euthanized for organ collection.

509 To evaluate immediate HRC4 biodistribution into lungs, one animal from the MeV-  
510 infection experiment (C1) was nebulized with 3 ml (4 mg/ml) immediately after euthanasia under  
511 mechanical ventilation (Dräger Primus anesthesia machine). For mid-term biodistribution, animals  
512 were nebulized 24 h (C2) or 16 h (C3) before euthanasia.

513

### 514 **Scintigraphy Gamma camera imaging of the aerosol delivery into NHP**

515 A study of the biodistribution of the nebulized aerosol was performed at the University of Tours,  
516 France. Following European recommendations, 2 five-year-old healthy female cynomolgus  
517 macaques, 3–4 kg, were housed under conventional conditions in the animal facility. The  
518 experimental protocol was conducted according to European regulations for animal  
519 experimentation and approved under the agreement reference MESR N°  
520 11682#2017100217166146. Animals were acclimatized to laboratory conditions and trained to  
521 breathe an aerosol with a facemask spontaneously. Aerosol generated from 3 ml of 0.9% NaCl  
522 mixed with 74 MBq of DTPA radiolabeled with technetium 99m ( $^{99m}\text{Tc-DTPA}$ ) was administered  
523 through a facemask connected to the prototype mesh nebulizers, as used in MeV infection  
524 experiments (Fig. 2a). Deposition of aerosol was extrapolated based on the  $^{99m}\text{Tc-DTPA}$  signal  
525 measured at the end of the nebulization using a gamma camera (Orbiter 75 Ecam, Siemens  
526 healthcare, Erlangen, Germany)<sup>68</sup>. The nebulizer charge was measured by counting the  
527 radioactivity in the syringe (that contained  $^{99m}\text{Tc-DTPA}$ ) before and after loading the nebulizers.  
528 Immediately after aerosol delivery, the animals were imaged using the gamma camera. The post-  
529 anterior static scintigraphy acquisition was performed for 120s. The amount of  $^{99m}\text{Tc-DTPA}$   
530 deposited into airways and stomach and remaining in the nebulizer was determined from the  
531 digitalized images taking into account the tissue attenuation coefficients, previously determined  
532 by perfusion scintigraphy (intravenous injection of  $^{99m}\text{Tc-macroaggregates}$  of albumin). The organ  
533 body outline was specified using a specific Region Of Interest (ROI), and the lungs were delineated  
534 using the perfusion scan ROI. The aerosol dose delivered to different organs of NHPs is reported  
535 as a percentage of the nominal dose placed in the nebulizer for that given experiment, taking into  
536 account the decay of technetium for all measurements.

537

### 538 **Peptide synthesis**

539 Unconjugated MeV HRC peptide and FIP (Carbobenzoxy-(Z)-D-Phe-L-Phe-Gly peptide) were  
540 purchased from Shanghai Ruifu Chemical Co., Ltd. Bis-maleimide cholesterol was custom made  
541 by Charnwood Molecular, Ltd. HRC4 and FIP-dimer cholesterol were conjugated and purified as  
542 previously described<sup>33</sup>. For the *in vivo* experiments in mice, HCR4 peptide was initially dissolved  
543 in DMSO to 50 mg/ml and stored at -80°C. Peptides were then diluted in water to reach either 0.1  
544 mg/kg or 1 mg/kg for intranasal administration. For nebulization of macaques, HRC4 peptide,  
545 soluble in water, was dissolved in Milli-Q water filtered to obtain a final concentration of 4 mg/ml.  
546 The pH of peptide solution was adjusted to 7 and stabilized using HEPES buffer. Peptide  
547 preparations were kept at 4°C for four days or at -80°C for the long-term storage.

548

### 549 **Fusion assay**

550 HEK 293T cells transfected with SLAM-coding plasmid and the omega reporter subunit of  $\beta$ -gal  
551 (“target cells”) were incubated with cells co-expressing viral glycoproteins (IC323 H and F) and  
552 the alpha reporter subunit of  $\beta$ -gal (“effector cells”) in the absence or presence of inhibitory  
553 peptides at the concentration of 5  $\mu$ M. In the absence of peptides, fusion between the target and  
554 effector cells permits reconstitution of  $\beta$ -galactosidase activity, quantified using the luminescence-  
555 based kit, Galacto-Star  $\beta$ -galactosidase reporter gene (ThermoFisher). Percent inhibition was  
556 calculated as the ratio of the relative luminescence units in the presence of a specific concentration  
557 of fusion inhibitory peptide and the relative luminescence units in the absence of inhibitor,  
558 corrected for background luminescence.

559

### 560 **Cell Toxicity Assay**

561 Vero cells were incubated at 37°C in the presence or absence of the indicated peptides at indicated  
562 concentrations up to 5  $\mu$ M HRC4 peptide as added into the media, and the cells were incubated a  
563 37°C. According to the manufacturer's guidelines, the viability was determined after 24 h using  
564 the Vybrant MTT (3-(4, 5-dimethylthiazolyl-2)-  
565 5-diphenyltetrazolium bromide) cell proliferation assay kit. TritonX-100 (1%) was used as a  
566 positive control. Absorbance was read at 540 nm using a Tecan M1000PRO microplate reader.

567

568 **Viral load quantification by RT-qPCR**

569 Viral RNA was extracted using Qiamap Viral RNA Kit (Qiagen) for sera and swabs samples and  
570 Nucleospin Kit (Macherey Nagel) for PBMCs. Viral load was evaluated by one-step RT-qPCR  
571 (NEB Luna® Universal One-Step RT-qPCR kit) using MeV-N-specific primers (MeV-N FW:  
572 GTG ATC AAA GTG AGA ATG AGC and MeV-N Rev: GCT GAC CTT CGA CTG TCC T)  
573 and GAPDH primers if necessary (GAPDH FW: CACCCACTCCTCCACCTTTGAC, GAPDH  
574 REV: GTCCACCACCCTGTTGCTGTAG). PCR amplification was recorded on a Step One plus  
575 apparatus (Thermo). All samples were run in duplicates, and results were analyzed using the ABI  
576 StepOne software v2.1 (Applied Biosystems).

577

578 **Laser diffraction measurement**

579 The aerodynamic performances of the aerosols generated by the prototype mesh nebulizer were  
580 determined by laser diffraction using a Spraytec™ instrument (Malvern Instruments Ltd.,  
581 Malvern, UK) and the Spraytec inhalation cell (Malvern Instruments Ltd., Malvern, UK)  
582 connected to an aspiration carried out by a vacuum pump set to 30-50L/min<sup>69</sup>. The prototype mesh  
583 nebulizers (n=4) were loaded with 3 ml of either NaCl 0.9% or the HCR4 peptide (4 mg/ml,  
584 dissolved as described above) and then connected to the inhalation cell. Nebulization duration was  
585 notified at the end of the complete aerosolization of the loaded 3 ml. Diffraction data and volume  
586 distribution were automatically registered by the Spraytec software. The volume mean diameter  
587 VMD, in  $\mu\text{m}$ , the respirable fractions inferior to 5  $\mu\text{m}$  ( $\% < 5 \mu\text{m}$ ) and inferior to 2  $\mu\text{m}$  ( $\% < 2 \mu\text{m}$ )  
588 were calculated by the software.

589 The output of nebulizer was determined by the difference between the weight of the  
590 nebulizer before and after nebulization and was expressed in percentage of the loaded volume. The  
591 output rate of each nebulizer (in ml/min) was then determined as the ratio between the output and  
592 the nebulization duration. At least, the residual volume corresponding to the volume of liquid  
593 remaining in the reservoir at the end of the nebulization was also determined by weighting the  
594 nebulizer before loading it and after nebulization.

595

596 **Enzyme-linked immunosorbent assay (ELISA)**

597 Determination of the HRC4 concentration in the serum and urine of macaques after the third  
598 nebulization was determined by ELISA. Maxisorp 96 well plates (Nunc) were coated overnight

599 with purified rabbit anti-MeV-F HRC antibodies (Genescript) ( $5 \mu\text{g/ml}$ ) in carbonate/bicarbonate  
600 buffer pH 9.2 at  $+4^\circ\text{C}$ . Plates were washed twice using PBS followed by incubation with 3% BSA  
601 in PBS (blocking buffer) for 60 min. Then, the blocking buffer was replaced with 2 dilutions of  
602 each sample in 3% PBS-BSA in duplicate and incubated for 90min at room temperature (RT).  
603 Wells were washed 3 times using PBS, and the peptide was detected using an HRP-conjugated  
604 rabbit custom-made anti-MeV F HRC antibody (1:1500) in blocking buffer for 2h at RT. Detection  
605 of HRP activity was measured by using the TMB substrate (Thermo) and reading absorbance at  
606 405 and 620nm on Multiskan FC reader (Thermo). The standard curves were established for each  
607 peptide, using the same ELISA conditions as for the test samples and the detection limit was  
608 determined to be 0.04nM.

609 Sera of MeV-infected NHPs were tested for the presence of anti-MeV antibodies by  
610 ELISA. Briefly, MeV nucleoprotein, produced as described previously<sup>70</sup> was coated onto 96-well  
611 ELISA plates overnight ( $1 \mu\text{g/well}$ ). Plates were blocked using a mix of PBS 1X-Milk 5% for 30  
612 min at room temperature. Serial dilutions (1/50 and then 1/3 serial dilutions until 1/2952450) were  
613 done in PBS 1X-Tween 0.05%-Milk and incubated 2h at RT. Secondary antibody goat anti-  
614 monkey IgG-A-M conjugated to horseradish peroxidase (HRP), (Sigma-Aldrich) was incubated  
615 for 1h at  $37^\circ$  and plates were revealed using TMB substrate solution (Thermo). Optical density  
616 was measured at 450 and 620nm using an ELISA reader (Thermo) and the absorbance difference  
617 between 450nm and 650nm was determined and corrected for blank readings. The serum sample  
618 is considered positive when its value is higher than three times the average value obtained with the  
619 negative sera of the same dilution and the results were expressed as reciprocal value of the last  
620 serum dilution giving the measurable values.

621

## 622 **Sero-neutralization**

623 Neutralizing Ab titers were determined using plaque reduction number test. Serial dilutions of sera  
624 (1:3) in DMEM medium containing 2% FCS were mixed with 50 PFU of MeV IC323-eGFP,  
625 incubated 30 min at  $37^\circ\text{C}$  and layered on Vero SLAM cells in 6 well-plates for 90 min. The inocula  
626 were replaced by DMEM 3% FBS / CMC 0.6% and plates were incubated for 3 days at  $37^\circ\text{C}$ .  
627 Plaques were counted after crystal violet staining, and relative neutralization titers were defined as  
628 the reciprocal dilutions of sera samples that completely inhibited the cytopathic effect of MeV.

629 Data were analyzed by Prism 8 software to calculate SN<sub>50</sub> values (non-linear regression, [inhibitor]  
630 vs. response, variable slope fitting).

631

### 632 **Immunofluorescence and histochemistry**

633 To assess the bioavailability of the HRC4 peptide on lungs, lung slices of paraffin embedded  
634 organs of 5µm thickness were stained and imaged by confocal microscopy as described previously  
635 <sup>24</sup>. Briefly, after being blocked and permeabilized in 0.1% TritonX100, 5% BSA solution, slices  
636 were sequentially incubated with a rabbit anti-HRC4 (Genscript) overnight at 4°C and with a  
637 secondary goat anti rabbit alexa-555 (Thermo) and DAPI for 1H at room temperature. Slides were  
638 imaged using a Zeiss LSM800 confocal microscope).

639 For hematoxylin-eosin staining, formalin-fixed tissues were processed and embedded in  
640 paraffin and tissue sections were then deparaffinized, rehydrated, rinsed, and placed in PBS before  
641 harrys hematoxylin staining (Diapath, diluted 1/3), washed with PBS and stained with eosin 1%  
642 (Sigma-Aldrich). Slide were washed with water dehydrated and mounted with DPX mounting  
643 medium (Sigma-Aldrich).

644

### 645 **Flow cytometry analysis**

646 Whole blood was collected on EDTA, then transferred into BD vacutainer CPT tubes (after  
647 removal of anticoagulant solution from CPT tubes) and spun at 2500g for 20 min. The PBMCs  
648 were collected and one-tenth were used to isolate RNA. The remaining cells were surface stained  
649 on ice using three different panels, including Panel A: CD150 BV-421 (clone A12, BD), CD8 AF  
650 647 (clone RPA-T8), CD20 APC-H7 (clone 2H7, BD), CD3 V500 (clone SP34-2, BD), CD14 Pe-  
651 cy7 (clone M5E2, BD); Panel B: CD150 BV421, CD3 V500, CCR7 Pe-Cy7 (clone G043H7,  
652 Biologend), CD8 AF647, CD45RA APC-H7 (clone 5H9, BD); and Panel C: CD150 BV421, IgD  
653 BV510 (clone IA6-2, BD), CD38 Pe-Cy7 (clone HB7, BD), CD27 AF647 (clone O323,  
654 Biologend), CD20 APC-H7. Cells were acquired on a MACSQuant®10 flow cytometer  
655 (Miltenyi).

656

### 657 **Statistical analysis**

658 We used the 2-way Anova analysis and Mantel Cox test for statistical analyses of results of the  
659 fusion test and animal survival and non-linear regression for the calculation of the serum



660 neutralization titer. We considered p-values of 0.05 or below (two-tailed tests) to be statistically  
661 significant. Statistical analyses were performed using GraphPad Prism 8 software.

662

663 **Acknowledgments:** We thank the animal experimentation team of Tours University for the  
664 realization of the animal experiments. We are grateful to Dr Cyrille Debard, (Biovelys,  
665 VetagroSup), Dr Guillaume Noel (Biovivo, VetagroSup) for helpful veterinary advices, to G.  
666 Gourru-Lesimple for the mycoplasma tests and all the members of the group Immunobiology of  
667 viral infection at CIRI for the help during the realisation of this study. We acknowledge the Servier  
668 Medical Art (smart.servier.com) for providing the images used for the schemas presented in the  
669 article and the contribution of the SFR Biosciences (UMS3444/CNRS, US8/Inserm, ENS de Lyon,  
670 UCBL) facility Lymic-Platim-Microscopy and AniRA PBES. The study was supported by Region  
671 ARA (project AerVirStop), by LABEX ECOFECT (ANR-11-LABX-0048) of Lyon University,  
672 within the program "Investissements d'Avenir" (ANR-11-IDEX-0007) operated by the French  
673 National Research Agency (ANR), and by ANR 16-ASMA-0008-01 to BH and by NIH (NS09126,  
674 NS105699 and AI159085) to MP.

675

676 **Author contributions:** Conceptualization: BH, OR, LV, MI, AM, MP, CM; Methodology: OR,  
677 CD, CG, MI, SLG, LV, JM, CM, ALG, CAA; Investigation: OR, LV, JM, MI, CD, CG, SLG, CM,  
678 LL, MF, YZ, DLP, GC, GR, AA; Funding acquisition: BH, MP; Project administration: BH, MP;  
679 Supervision: BH, OR, CD, MI, CM; Writing – original draft: OR, MI, BH; Writing – review &  
680 editing: OR, BH, MI, MP, AM.

681 **Competing interests:**

682 S. Le Guellec is employed by DTF Medical (Saint Etienne, France) and L. Vecellio was employed  
683 by DTF Medical from 2001 to 2018 and by Nemera (La Verpilliere, France) from 2018 to 2020.

684 **Data availability:** All data are available in the paper or the Supplementary materials.

685

686

687

688 **References**

- 689 1. Anderson, R. M. & May, R. M. Directly transmitted infections diseases: control by  
690 vaccination. *Science* **215**, 1053–1060 (1982).
- 691 2. Patel, M. K. Progress Toward Regional Measles Elimination — Worldwide, 2000–2019.  
692 *MMWR Morb Mortal Wkly Rep* **69**, (2020).
- 693 3. Durrheim, D. N. *et al.* A dangerous measles future looms beyond the COVID-19 pandemic.  
694 *Nat Med* **27**, 360–361 (2021).
- 695 4. Mazidimoradi, A. & Salehiniya, H. Decreased vaccination coverage and recurrence risk of  
696 measles due to COVID-19 pandemic. *EXCLI J* **20**, 1367–1369 (2021).
- 697 5. Roberts, L. Why measles deaths are surging - and coronavirus could make it worse. *Nature*  
698 **580**, 446–447 (2020).
- 699 6. Dixon, M. G. *et al.* Progress Toward Regional Measles Elimination - Worldwide, 2000-2020.  
700 *MMWR Morb Mortal Wkly Rep* **70**, 1563–1569 (2021).
- 701 7. Ferren, M., Horvat, B. & Mathieu, C. Measles Encephalitis: Towards New Therapeutics.  
702 *Viruses* **11**, 1017 (2019).
- 703 8. Lemon, K. *et al.* Early target cells of measles virus after aerosol infection of non-human  
704 primates. *PLoS Pathog* **7**, e1001263 (2011).
- 705 9. Lin, W.-H. W., Tsay, A. J., Lalime, E. N., Pekosz, A. & Griffin, D. E. Primary differentiated  
706 respiratory epithelial cells respond to apical measles virus infection by shedding  
707 multinucleated giant cells. *Proc Natl Acad Sci U S A* **118**, e2013264118 (2021).
- 708 10. Ludlow, M., McQuaid, S., Milner, D., Swart, R. L. de & Duprex, W. P. Pathological  
709 consequences of systemic measles virus infection. *The Journal of Pathology* **235**, 253–265  
710 (2015).
- 711 11. Laksono, B. M. *et al.* Measles skin rash: Infection of lymphoid and myeloid cells in the dermis  
712 precedes viral dissemination to the epidermis. *PLOS Pathogens* **16**, e1008253 (2020).
- 713 12. Gourru-Lesimple, G. *et al.* Measles virus infection of human keratinocytes: Possible link  
714 between measles and atopic dermatitis. *J Dermatol Sci* **86**, 97–105 (2017).
- 715 13. Rota, P. A. *et al.* Measles. *Nat Rev Dis Primers* **2**, 16049 (2016).
- 716 14. Hippee, C. E. *et al.* Measles virus exits human airway epithelia within dislodged metabolically  
717 active infectious centers. *PLoS Pathog* **17**, e1009458 (2021).
- 718 15. Griffin, D. E. Measles immunity and immunosuppression. *Curr Opin Virol* **46**, 9–14 (2021).
- 719 16. Kerdiles, Y. M., Sellin, C. I., Druelle, J. & Horvat, B. Immunosuppression caused by measles  
720 virus: role of viral proteins. *Rev. Med. Virol.* **16**, 49–63 (2006).
- 721 17. Swart, R. L. de *et al.* Predominant Infection of CD150+ Lymphocytes and Dendritic Cells  
722 during Measles Virus Infection of Macaques. *PLOS Pathogens* **3**, e178 (2007).
- 723 18. Tatsuo, H., Ono, N., Tanaka, K. & Yanagi, Y. SLAM (CDw150) is a cellular receptor for  
724 measles virus. *Nature* **406**, 893–897 (2000).
- 725 19. de Witte, L., Abt, M., Schneider-Schaulies, S., van Kooyk, Y. & Geijtenbeek, T. B. H. Measles  
726 virus targets DC-SIGN to enhance dendritic cell infection. *J Virol* **80**, 3477–3486 (2006).

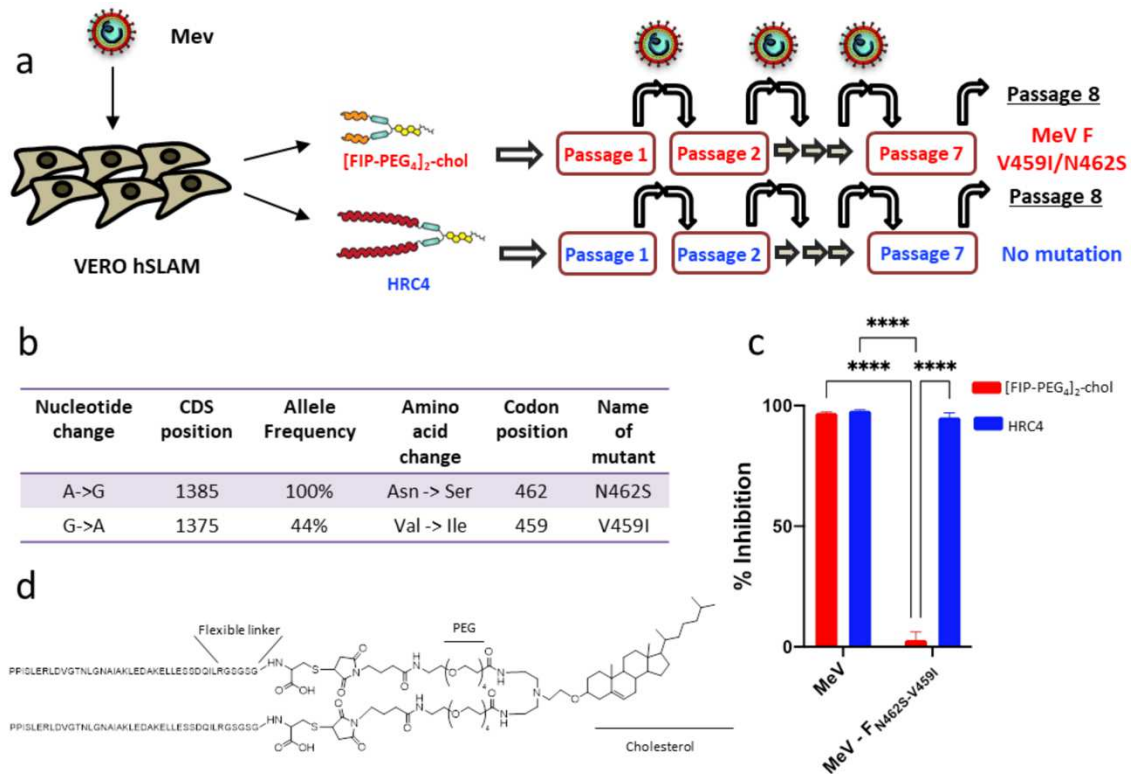
- 727 20. Delpout, S. *et al.* Nectin-4 Interactions Govern Measles Virus Virulence in a New Model of  
728 Pathogenesis, the Squirrel Monkey (*Saimiri sciureus*). *J Virol* **91**, e02490-16 (2017).
- 729 21. Singh, B. K. *et al.* Cell-to-Cell Contact and Nectin-4 Govern Spread of Measles Virus from  
730 Primary Human Myeloid Cells to Primary Human Airway Epithelial Cells. *J Virol* **90**, 6808–  
731 6817 (2016).
- 732 22. Shirogane, Y. *et al.* CADM1 and CADM2 Trigger Neuropathogenic Measles Virus-Mediated  
733 Membrane Fusion by Acting in cis. *J Virol* **95**, e0052821 (2021).
- 734 23. Harrison, S. C. Viral membrane fusion. *Virology* **0**, 498–507 (2015).
- 735 24. Welsch, J. C. *et al.* Fatal measles virus infection prevented by brain-penetrant fusion inhibitors.  
736 *J Virol* **87**, 13785–13794 (2013).
- 737 25. Mathieu, C. *et al.* Prevention of measles virus infection by intranasal delivery of fusion  
738 inhibitor peptides. *J Virol* **89**, 1143–1155 (2015).
- 739 26. Bodier-Montagutelli, E. *et al.* Protein stability during nebulization: Mind the collection step!  
740 *Eur J Pharm Biopharm* **152**, 23–34 (2020).
- 741 27. Hertel, S. P., Winter, G. & Friess, W. Protein stability in pulmonary drug delivery via  
742 nebulization. *Adv Drug Deliv Rev* **93**, 79–94 (2015).
- 743 28. Pritchard, J. N., Hatley, R. H., Denyer, J. & Hollen, D. von. Mesh nebulizers have become the  
744 first choice for new nebulized pharmaceutical drug developments. *Ther Deliv* **9**, 121–136  
745 (2018).
- 746 29. de Vries, R. D. *et al.* Measles immune suppression: lessons from the macaque model. *PLoS*  
747 *Pathog* **8**, e1002885 (2012).
- 748 30. Larder, B. A., Kemp, S. D. & Purifoy, D. J. Infectious potential of human immunodeficiency  
749 virus type 1 reverse transcriptase mutants with altered inhibitor sensitivity. *Proc Natl Acad Sci*  
750 *U S A* **86**, 4803–4807 (1989).
- 751 31. Hashimoto, K. *et al.* SLAM (CD150)-Independent Measles Virus Entry as Revealed by  
752 Recombinant Virus Expressing Green Fluorescent Protein. *J Virol* **76**, 6743–6749 (2002).
- 753 32. Richardson, C. D., Scheid, A. & Choppin, P. W. Specific inhibition of paramyxovirus and  
754 myxovirus replication by oligopeptides with amino acid sequences similar to those at the N-  
755 termini of the F1 or HA2 viral polypeptides. *Virology* **105**, 205–222 (1980).
- 756 33. Bovier, F. T. *et al.* Inhibition of Measles Viral Fusion Is Enhanced by Targeting Multiple  
757 Domains of the Fusion Protein. *ACS Nano* (2021) doi:10.1021/acsnano.1c02057.
- 758 34. Ha, M. N. *et al.* Mutations in the Fusion Protein of Measles Virus That Confer Resistance to  
759 the Membrane Fusion Inhibitors Carbobenzoxy-d-Phe-l-Phe-Gly and 4-Nitro-2-Phenylacetyl  
760 Amino-Benzamide. *J Virol* **91**, e01026-17 (2017).
- 761 35. Sellin, C. I. *et al.* Interplay between virus-specific effector response and Foxp3 regulatory T  
762 cells in measles virus immunopathogenesis. *PLoS One* **4**, e4948 (2009).
- 763 36. Druelle, J., Sellin, C. I., Waku-Kouomou, D., Horvat, B. & Wild, F. T. Wild type measles virus  
764 attenuation independent of type I IFN. *Virol J* **5**, 22 (2008).
- 765 37. Welsch, J. C. *et al.* Fatal measles virus infection prevented by brain-penetrant fusion inhibitors.  
766 *J. Virol.* **87**, 13785–13794 (2013).

- 767 38. Cunningham, S. *et al.* Nebulised ALX-0171 for respiratory syncytial virus lower respiratory  
768 tract infection in hospitalised children: a double-blind, randomised, placebo-controlled, phase  
769 2b trial. *The Lancet Respiratory Medicine* **9**, 21–32 (2021).
- 770 39. Abughazaleh, R. D. & Tracy, T. S. Therapeutic Index. in *Wiley Encyclopedia of Clinical Trials*  
771 (eds. D’Agostino, R. B., Sullivan, L. & Massaro, J.) eoct322 (John Wiley & Sons, Inc., 2007).  
772 doi:10.1002/9780471462422.eoct322.
- 773 40. Park, H.-K. *et al.* Reference values of clinical pathology parameters in cynomolgus monkeys  
774 (*Macaca fascicularis*) used in preclinical studies. *Lab Anim Res* **32**, 79–86 (2016).
- 775 41. Bennett, J. S., Gossett, K. A., McCarthy, M. P. & Simpson, E. D. Effects of ketamine  
776 hydrochloride on serum biochemical and hematologic variables in rhesus monkeys (*Macaca*  
777 *mulatta*). *Vet Clin Pathol* **21**, 15–18 (1992).
- 778 42. CIDER, C. for D. E. and R. Estimating the Maximum Safe Starting Dose in Initial Clinical  
779 Trials for Therapeutics in Adult Healthy Volunteers. *U.S. Food and Drug Administration*  
780 [https://www.fda.gov/regulatory-information/search-fda-guidance-documents/estimating-](https://www.fda.gov/regulatory-information/search-fda-guidance-documents/estimating-maximum-safe-starting-dose-initial-clinical-trials-therapeutics-adult-healthy-volunteers)  
781 [maximum-safe-starting-dose-initial-clinical-trials-therapeutics-adult-healthy-volunteers](https://www.fda.gov/regulatory-information/search-fda-guidance-documents/estimating-maximum-safe-starting-dose-initial-clinical-trials-therapeutics-adult-healthy-volunteers)  
782 (2018).
- 783 43. Fröhlich, E., Mercuri, A., Wu, S. & Salar-Behzadi, S. Measurements of Deposition, Lung  
784 Surface Area and Lung Fluid for Simulation of Inhaled Compounds. *Front Pharmacol* **7**, 181  
785 (2016).
- 786 44. Beck, S. E. *et al.* Deposition and Expression of Aerosolized rAAV Vectors in the Lungs of  
787 Rhesus Macaques. *Molecular Therapy* **6**, 546–554 (2002).
- 788 45. Hyde, D. M., Tyler, N. K., Putney, L. F., Singh, P. & Gundersen, H. J. G. Total number and  
789 mean size of alveoli in mammalian lung estimated using fractionator sampling and unbiased  
790 estimates of the Euler characteristic of alveolar openings. *Anat Rec A Discov Mol Cell Evol*  
791 *Biol* **277**, 216–226 (2004).
- 792 46. El Mubarak, H. S. *et al.* Infection of cynomolgus macaques (*Macaca fascicularis*) and rhesus  
793 macaques (*Macaca mulatta*) with different wild-type measles viruses. *J Gen Virol* **88**, 2028–  
794 2034 (2007).
- 795 47. de Vries, R. D. *et al.* In vivo tropism of attenuated and pathogenic measles virus expressing  
796 green fluorescent protein in macaques. *J Virol* **84**, 4714–4724 (2010).
- 797 48. Giudice, E. L. & Campbell, J. D. Needle-free vaccine delivery. *Adv Drug Deliv Rev* **58**, 68–  
798 89 (2006).
- 799 49. Orenius, T., LicPsych, Säilä, H., Mikola, K. & Ristolainen, L. Fear of Injections and Needle  
800 Phobia Among Children and Adolescents: An Overview of Psychological, Behavioral, and  
801 Contextual Factors. *SAGE Open Nursing* **4**, 2377960818759442 (2018).
- 802 50. Wright, S., Yelland, M., Heathcote, K., Ng, S.-K. & Wright, G. Fear of needles--nature and  
803 prevalence in general practice. *Aust Fam Physician* **38**, 172–176 (2009).
- 804 51. Carlsson, H.-E., Schapiro, S. J., Farah, I. & Hau, J. Use of primates in research: A global  
805 overview. *American Journal of Primatology* **63**, 225–237 (2004).

- 806 52. Gardner, M. B. & Luciw, P. A. Macaque Models of Human Infectious Disease. *ILAR Journal*  
807 **49**, 220–255 (2008).
- 808 53. O’Neil, R. M., Ashack, R. J. & Goodman, F. R. A comparative study of the respiratory  
809 responses to bronchoactive agents in rhesus and cynomolgus monkeys. *Journal of*  
810 *Pharmacological Methods* **5**, 267–273 (1981).
- 811 54. Dubus, J. C. *et al.* Aerosol deposition in neonatal ventilation. *Pediatr Res* **58**, 10–14 (2005).
- 812 55. J, M. *et al.* Optimization and Dose Estimation of Aerosol Delivery to Non-Human Primates.  
813 *Journal of Aerosol Medicine and Pulmonary Drug Delivery* (2016)  
814 doi:10.1089/jamp.2015.1250.
- 815 56. Rosenberg, Y. J. & Fink, J. B. Creation of a protective pulmonary bioshield against inhaled  
816 organophosphates using an aerosolized bioscavenger. *Ann N Y Acad Sci* **1374**, 151–158  
817 (2016).
- 818 57. McPhee, F. *et al.* Virological escape in HCV genotype-1-infected patients receiving  
819 daclatasvir plus ribavirin and peginterferon alfa-2a or alfa-2b. *Antivir Ther* **19**, 479–490  
820 (2014).
- 821 58. Auwaerter, P. G. *et al.* Measles virus infection in rhesus macaques: altered immune responses  
822 and comparison of the virulence of six different virus strains. *J Infect Dis* **180**, 950–958 (1999).
- 823 59. Marty, F. M. *et al.* A Phase 2b, Randomized, Double-blind, Placebo-Controlled Multicenter  
824 Study Evaluating Antiviral Effects, Pharmacokinetics, Safety, and Tolerability of Presatovir  
825 in Hematopoietic Cell Transplant Recipients with Respiratory Syncytial Virus Infection of the  
826 Lower Respiratory Tract. *Clin Infect Dis* **71**, 2787–2795 (2020).
- 827 60. Mathieu, C. *et al.* Molecular Features of the Measles Virus Viral Fusion Complex That Favor  
828 Infection and Spread in the Brain. *mBio* **12**, e00799-21 (2021).
- 829 61. Pessi, A. *et al.* A general strategy to endow natural fusion-protein-derived peptides with potent  
830 antiviral activity. *PloS One* **7**, e36833 (2012).
- 831 62. Figueira, T. N. *et al.* In Vivo Efficacy of Measles Virus Fusion Protein-Derived Peptides Is  
832 Modulated by the Properties of Self-Assembly and Membrane Residence. *Journal of Virology*  
833 **91**, (2017).
- 834 63. de Vries, R. D. *et al.* Intranasal fusion inhibitory lipopeptide prevents direct-contact SARS-  
835 CoV-2 transmission in ferrets. *Science* **371**, 1379–1382 (2021).
- 836 64. Outlaw, V. K. *et al.* Inhibition of Coronavirus Entry In Vitro and Ex Vivo by a Lipid-  
837 Conjugated Peptide Derived from the SARS-CoV-2 Spike Glycoprotein HRC Domain. *mBio*  
838 **11**, e01935-20 (2020).
- 839 65. Mathieu, C., Porotto, M., Figueira, T. N., Horvat, B. & Moscona, A. Fusion Inhibitory  
840 Lipopeptides Engineered for Prophylaxis of Nipah Virus in Primates. *J Infect Dis* **218**, 218–  
841 227 (2018).
- 842 66. Radecke, F. *et al.* Rescue of measles viruses from cloned DNA. *EMBO J* **14**, 5773–5784  
843 (1995).

- 844 67. Greninger, A. L. *et al.* Rapid Metagenomic Next-Generation Sequencing during an  
845 Investigation of Hospital-Acquired Human Parainfluenza Virus 3 Infections. *Journal of*  
846 *Clinical Microbiology* **55**, 177–182 (2017).
- 847 68. Respaud, R. *et al.* Development of a drug delivery system for efficient alveolar delivery of a  
848 neutralizing monoclonal antibody to treat pulmonary intoxication to ricin. *J Control Release*  
849 **234**, 21–32 (2016).
- 850 69. Lelong, N., Junqua-Moulet, A., Diot, P. & Vecellio, L. Comparison of laser diffraction  
851 measurements by Mastersizer X and Spraytec to characterize droplet size distribution of  
852 medical liquid aerosols. *J Aerosol Med Pulm Drug Deliv* **27**, 94–102 (2014).
- 853 70. Kerdiles, Y. M. *et al.* Immunomodulatory properties of morbillivirus nucleoproteins. *Viral*  
854 *Immunol.* **19**, 324–334 (2006).
- 855
- 856

## Figures and figure legends

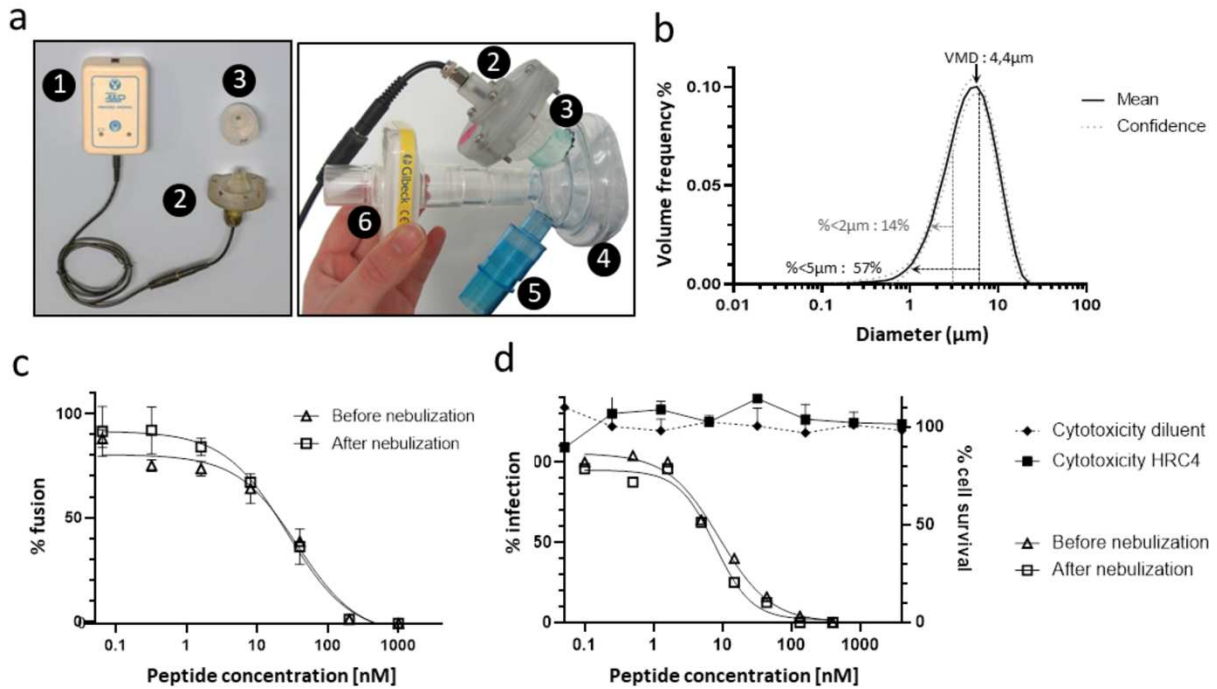


858

859

860 **Fig. 1. HRC4 lipopeptide treatment does not generate MeV escape variants.** (a) Schematic  
 861 presentation of viral passaging. MeV IC323-eGFP was serially passaged 8 times on the Vero  
 862 SLAM cells in presence of either 1  $\mu$ M [FIP-PEG<sub>4</sub>]<sub>2</sub>-chol or HRC4 peptide, added to the culture  
 863 after the infection. Virus was titrated after each passage and 100 PFU used for each subsequent  
 864 infection. Sequencing of viral RNA after the 8<sup>th</sup> passage revealed two mutations in the F-HRC  
 865 domain for the infection done in the presence of [FIP-PEG<sub>4</sub>]<sub>2</sub>-chol: V459I and N462S, while no  
 866 mutations in the presence of HRC4 peptide were found. (b) The most frequent mutation events in  
 867 F after MeV IC323 was serially passaged 8 times on the Vero SLAM cells in presence of [FIP-  
 868 PEG<sub>4</sub>]<sub>2</sub>-chol. (c) Inhibition of cell-cell fusion mediated by MeV F bearing the indicated mutations  
 869 by either 5  $\mu$ M [FIP-PEG<sub>4</sub>]<sub>2</sub>-chol or HRC4 peptide, using HEK-293T cells transfected with SLAM  
 870 and the omega reporter subunit of  $\beta$ -gal, incubated with cells co-expressing viral glycoproteins  
 871 (IC323 H and F) and the alpha reporter subunit of  $\beta$ -gal (\*\*\*\* p<0,001, Two-Way ANOVA  
 872 analysis). (d) Schematic of the HRC4 lipopeptide, used in the further study.

873



874

875

876

877 **Fig. 2. Utilization of the prototype mesh nebulizer with low Volume Medium Diameter**

878 **preserves functional activity of HRC4 lipopeptide.** (a) Composition of the prototype mesh

879 nebulizer used in experiments: 1. electronic controller; 2. piezo-electric vibrator; 3. reservoir

880 containing the mesh; 4. facemask; 5. one-way inspiratory valve; 6. absolute filter. (b) Graphical

881 representation of particle size distribution obtained from laser diffraction analysis of aerosolized

882 3ml of HRC4 lipopeptide. Plain line presents the mean values of four nebulizers used in the study

883 and dotted line standard deviation. Percentage of particles  $< 5\mu\text{m}$  and  $< 2\mu\text{m}$  present the fraction

884 of aerosol below the indicated size, corresponding to the aerosol penetrating into either lung in

885 general ( $< 5\mu\text{m}$ ) or into alveolar regions of lungs ( $< 2\mu\text{m}$ ). Volume Mean Diameter (VMD)

886 presents the mean size of generated aerosols. (c) Fusion inhibitory activity of HRC4, measured

887 before or after peptide nebulization, using  $\beta$ -gal complementation assay. (d) Antiviral activity of

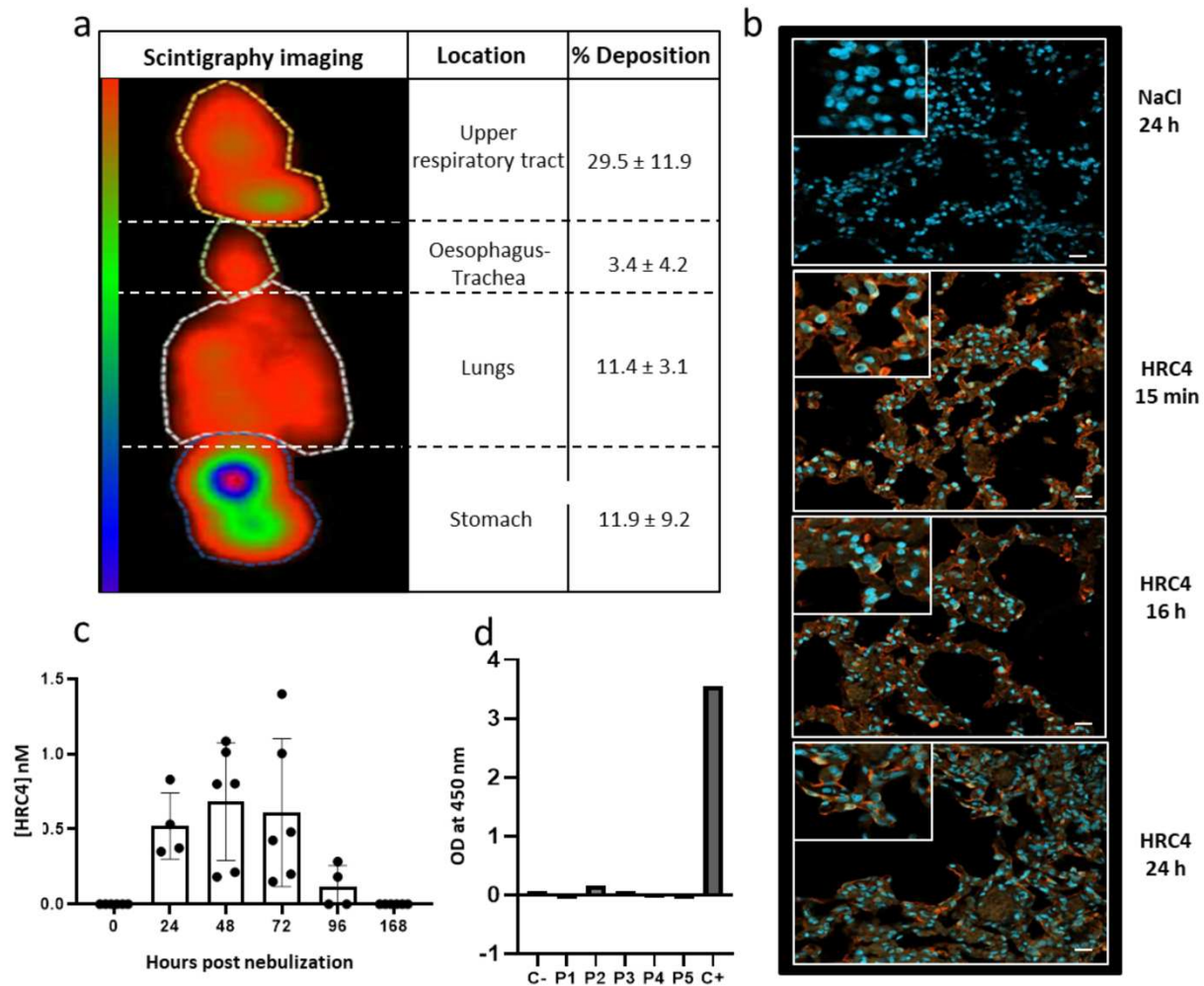
888 HRC4 measured prior and after nebulization, determined by  $\text{IC}_{50}$  measurement using plaque

889 reduction assay on Vero-hSLAM cells, and cytotoxicity assay, performed by assessing of cells

890 viability after 96 h by MTT assay.

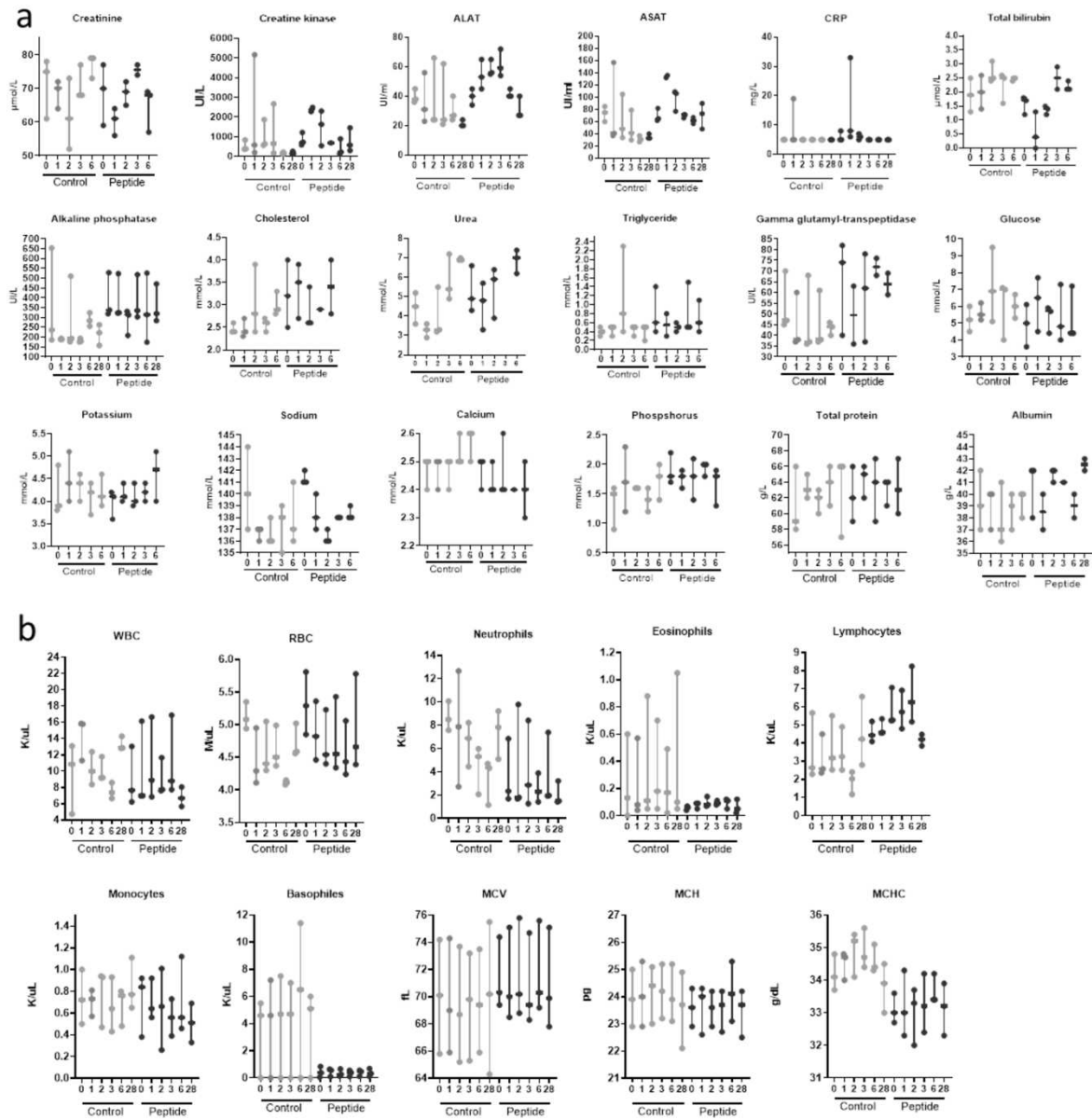
891





892

893 **Fig. 3. Delivery of the aerosol into macaques' lungs.** (a) Representative scintigraphy imaging  
 894 of different regions of interest in a cynomolgus monkeys nebulized with  $^{99m}\text{TC}$ -DTPA tracer (74  
 895 Mbq) in 3 ml NaCl 0.9%, using a prototype mesh nebulizer and measured by E-cam gamma  
 896 camera. Mean values  $\pm$ SD of the distribution of aerosol deposition were determined from the  
 897 digitalized images obtained in four experiments. (b) Lung localization of the aerosolized HRC4  
 898 peptide analyzed in cranial lobe lung sections from monkeys nebulized under mechanical  
 899 ventilation for the indicated time: 15 min (n=1), 24 h (n=2) or 16 h (n=1), prior to euthanasia.  
 900 Staining was performed with rabbit anti-HRC peptide and goat anti-rabbit Alexa 555 (orange  
 901 staining) and DAPI was used to stain nuclei (blue staining) (Scale bar: 20 $\mu\text{m}$ ). (c) Quantification  
 902 of HRC4 in the NHPs' serum after peptide nebulization, by ELISA. (d) Determination of the  
 903 presence of anti-HRC4 antibodies (IgG, IgA and IgM) by ELISA in the serum of peptide-nebulized  
 904 macaques, from either HRC4 biodistribution or MeV-infection study (values obtained at day 0 are  
 905 subtracted from those at D28 for each individual animal). Negative control (C-) corresponds to  
 906 serum of a naïve macaque and positive control (C+) to rabbit anti-HRC4 antiserum.



907

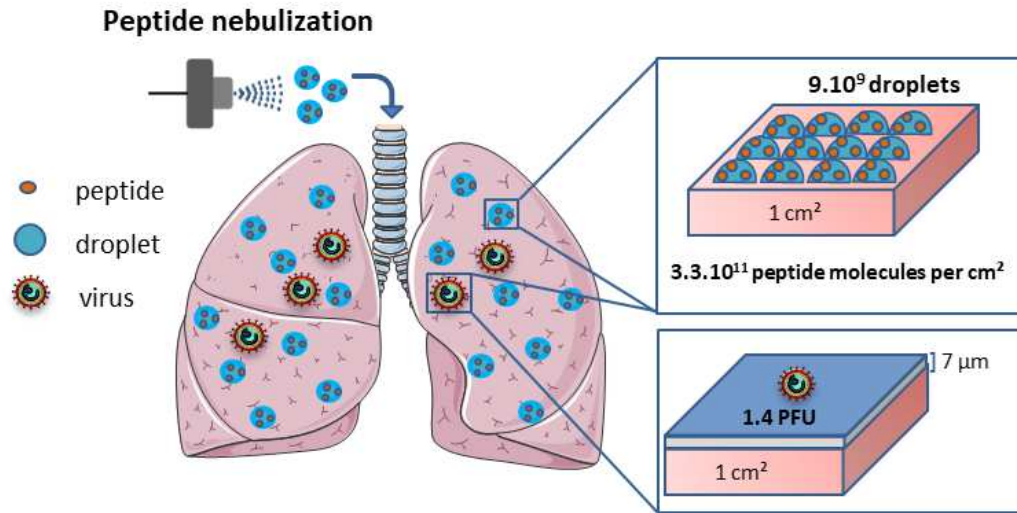
908 **Fig. 4. Evolution of biochemical (a) and hematological (b) parameters in blood of cynomolgus**  
 909 **monkeys following nebulization of either saline (control) or HRC4 (peptide).** (a)

910 Concentration of indicated biochemical parameters in blood of monkeys, measured on days 0, 1,  
 911 2, 3, 6 and 28 after nebulization of either saline solution (0.9% NaCl, n=3) or HRC4 peptide (4  
 912 mg/kg, n=5); (b) Haematological parameters measured at days 0, 1, 2, 3, 6 and 28 after nebulisation

913 of either saline solution (0.9% NaCl, n=3) or HRC4 peptide (4 mg/kg, n=5). ALAT: Alanine  
 914 aminotransferase; ASAT: Aspartate aminotransferase; CRP: C-reactive protein; MCV: Mean  
 915 corpuscular volume; WBC: white blood cells; RBC: red blood cells; MCH: Mean corpuscular;  
 916 MCHC: Mean corpuscular haemoglobin concentration.

917

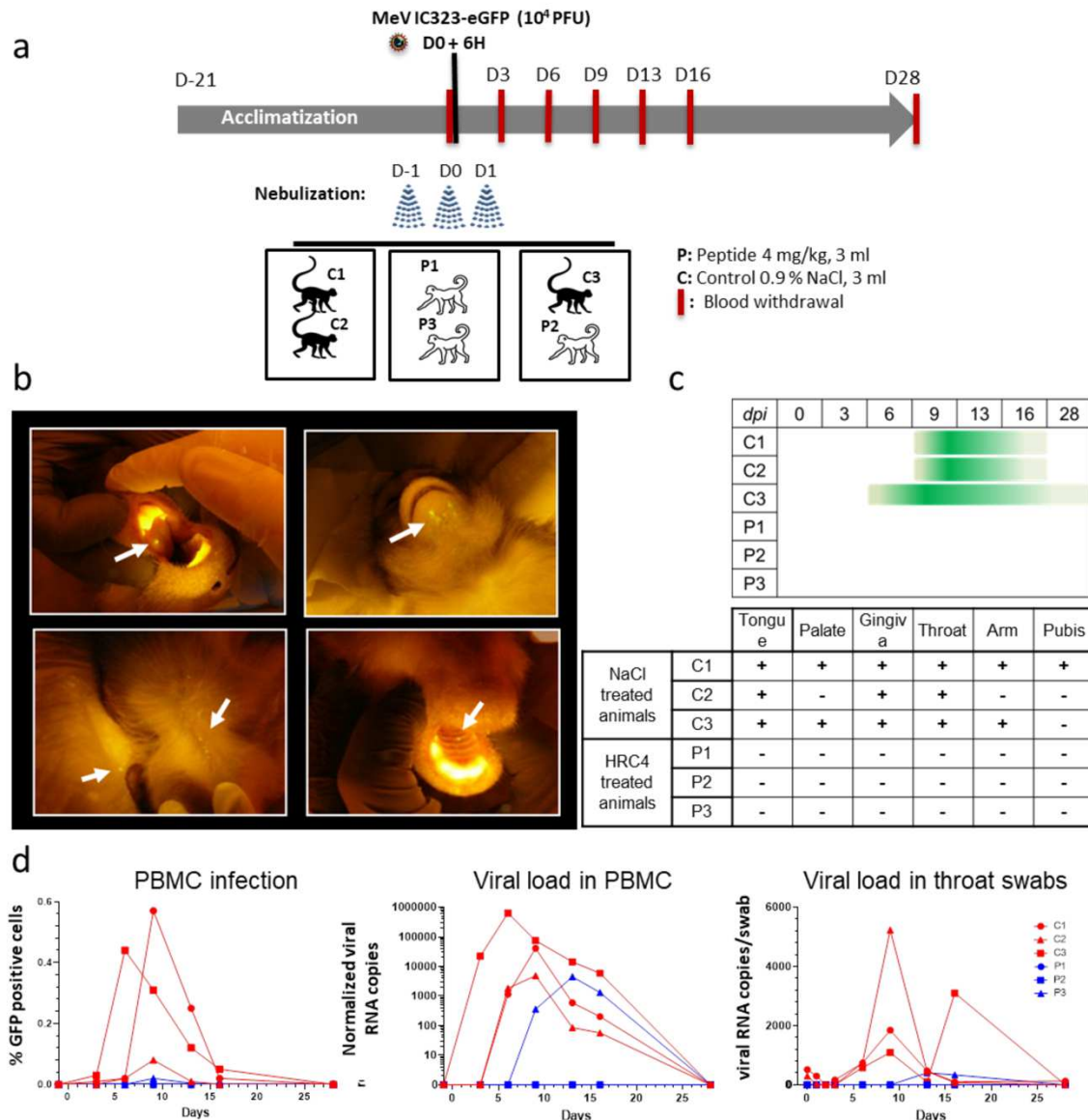
918  
919  
920



921  
922  
923

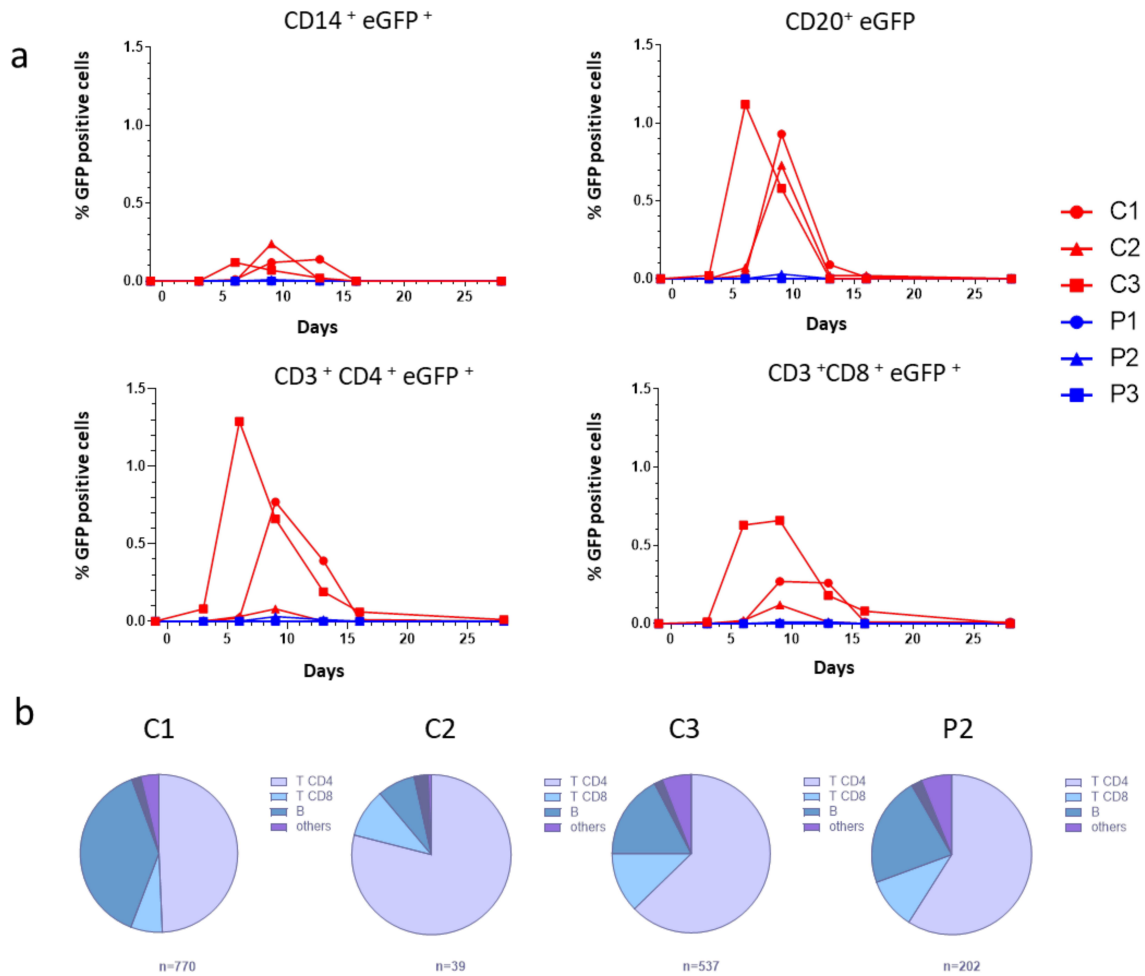
924 **Fig. 5. Schematic presentation of the peptide and virus deposition in the lungs.** The calculation  
925 based on the estimation of the peptide dose per unit of lung internal surface, taking into  
926 consideration the number of droplets formed following the administration and the peptide  
927 molecules into the pulmonary area. Following the nebulization, 11% of the formed droplets  
928 reached the lungs (as shown in Fig 1A), representing a density of  $9 \times 10^9$  droplets/cm<sup>2</sup> of lung  
929 internal surface and containing  $3 \times 10^{11}$  peptide molecules/cm<sup>2</sup>. Instillation of the viral inoculum  
930 ( $10^4$  Plaque Forming Units, PFU in 5 ml) via endotracheal tube leads to the virus dispersion in the  
931 lung conductive airways in the form of 7 µm thin liquid layer (presented in blue color, covering  
932 the maximum surface of 7140 cm<sup>2</sup>). This represents 3.5 % of the total lung surface area, giving the  
933 density of infectious particles of 1.4 PFU per cm<sup>2</sup> of airways and estimated ratio between the  
934 peptide and the virus is  $2 \times 10^{11}$  per cm<sup>2</sup> of the lung surface.

935  
936  
937  
938  
939



940

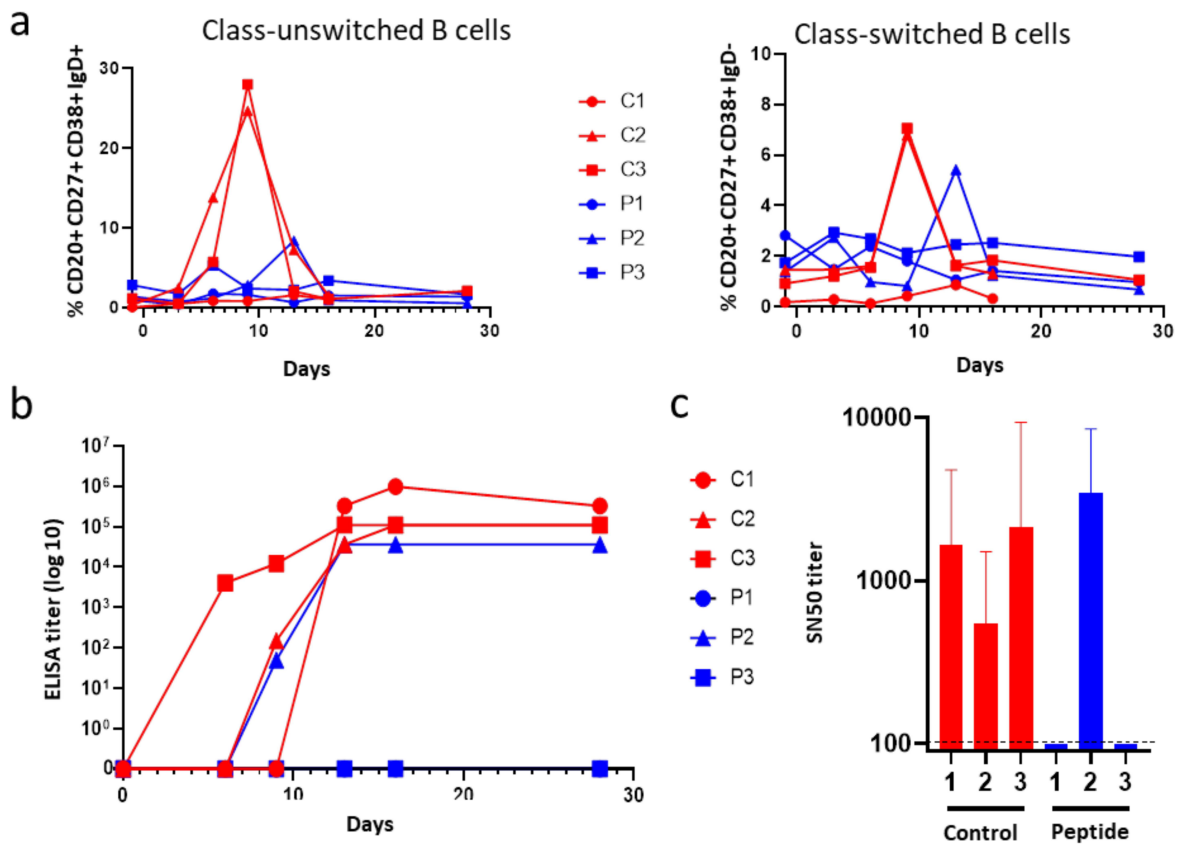
941 **Fig. 6. HRC4 nebulization protects monkeys from clinical manifestation of MeV**  
 942 **infection.** (a) Experimental design: cynomolgus monkeys (3 animals/group) were either nebulized  
 943 with 3 ml of NaCl 0.9% (control group, C) or with 3 ml HRC4 peptide 4 mg/ml (experimental  
 944 group, P), 24 h and 6 h before and 24 h after intra-tracheal infection with  $10^4$  PFU MeV IC323  
 945 eGFP. Blood samples were taken every 3 days for the first 16 days and fluorescence of the skin  
 946 and mucosa tested at that time points. (b) Macroscopic manifestation of MeV infection, typical  
 947 fluorescent rash observed on tongue, skin (back and chin) and palate (marked with white arrows),  
 948 monitored under anesthesia using a blue light with orange filter. (c) Duration of the clinical signs  
 949 in MeV-infected animals followed daily (dpi: days post infection). (d) Analysis of viremia by  
 950 quantification of the percentage of GFP<sup>+</sup> peripheral blood mononuclear cells (PBMC) in the blood  
 951 by flow cytometry and MeV-specific RNA in PBMCs and in throat swabs by RT-qPCR, during  
 952 the course of infection.



953

954

955 **Fig. 7. Nebulization of HRC4 peptide protects PBMCs from MeV infection.** (a) Quantification  
 956 of MeV eGFP positive cells in indicated PBMC subpopulations by flow cytometry: CD14<sup>+</sup>  
 957 monocytes, CD4<sup>+</sup>, CD8<sup>+</sup> and CD20<sup>+</sup> lymphocytes in MeV-infected cynomolgus monkeys by flow  
 958 cytometry, following the nebulization of either 0.9% NaCl (C) or HRC4 peptide (P). CD4<sup>+</sup> T  
 959 lymphocytes were characterized as CD3<sup>+</sup>CD8<sup>-</sup>, and CD8<sup>+</sup> T lymphocytes were characterized as  
 960 CD3<sup>+</sup>/CD8<sup>+</sup>; B-lymphocytes were characterized as CD3<sup>-</sup>/CD20<sup>+</sup> cells. (b) Analysis of the  
 961 contribution of each lymphocyte subpopulation among infected PBMCs; results are presented as  
 962 the percentage of each analyzed cell population among the infected cells on the day of peak of  
 963 MeV infection (day 6 for C3 and day 9 for C1, C2 and P2). Numbers below the graphs correspond  
 964 to the number of analyzed cells for each presented animal. Data were acquired on a MACSQuant®  
 965 10 flow cytometer (Miltenyi).



966

967 **Fig. 8. Establishment of the humoral immune response in animals that develop MeV**

968 **infection. (a)** Analysis of the presence of class-unswitched IgM secreting B cells (CD20<sup>+</sup> CD27<sup>+</sup>

969 CD38<sup>+</sup> IgD<sup>+</sup>) and switched memory B cells secreting IgG, IgA or IgE (CD20<sup>+</sup> CD27<sup>+</sup> CD38<sup>+</sup> IgD<sup>-</sup>

970 ) in the peripheral blood of NHPs, in following the nebulization of either 0,85% NaCl (C) or HRC4

971 peptide (P) and MeV infection; **(b)** Quantification of total MeV-specific immunoglobulin by

972 ELISA; plotted values present the reciprocal values of last serum dilution with detectable optical

973 density measure. **(c)** Sero-neutralization assay performed using plaque reduction test, following

974 the infection of Vero-hSLAM cells with MeV IC323-eGFP (50 PFU/well). SN<sub>50</sub> values were

975 calculated by regression using Prism software (Nonlinear fitting, variable slope, R<sup>2</sup>: 0.87-0.98);

976 dashed line represents detection limit and error bars represent confidence interval, variable slope,

977 R<sup>2</sup>: 0.87-0.98); dashed line presents detection limit.

## Supplementary Files

This is a list of supplementary files associated with this preprint. Click to download.

- [ReynardSupplementary.pdf](#)